gels

MDPI

Article

Development of Flexible Plasticized Ion Conducting Polymer Blend Electrolytes Based on Polyvinyl Alcohol (PVA): Chitosan (CS) with High Ion Transport Parameters Close to Gel Based Electrolytes

Niyaz M. Sadiq [1], Shujahadeen B. Aziz [1,2,*] and Mohd F. Z. Kadir [3]

[1] Hameed Majid Advanced Polymeric Materials Research Lab., Physics Department, College of Science, University of Sulaimani, Qlyasan Street, Sulaimani 46001, Iraq; niyaz.sadiq@univsul.edu.iq
[2] Department of Civil Engineering, College of Engineering, Komar University of Science and Technology, Sulaimani 46001, Iraq
[3] Centre for Foundation Studies in Science, University of Malaya, Kuala Lumpur 50603, Malaysia; mfzkadir@um.edu.my
* Correspondence: shujahadeenaziz@gmail.com

Abstract: In the current study, flexible films of polyvinyl alcohol (PVA): chitosan (CS) solid polymer blend electrolytes (PBEs) with high ion transport property close enough to gel based electrolytes were prepared with the aid of casting methodology. Glycerol (GL) as a plasticizer and sodium bromide (NaBr) as an ionic source provider are added to PBEs. The flexible films have been examined for their structural and electrical properties. The GL content changed the brittle and solid behavior of the films to a soft manner. X-ray diffraction (XRD) and Fourier transform infrared (FTIR) methods were used to examine the structural behavior of the electrolyte films. X-ray diffraction investigation revealed that the crystalline character of PVA:CS:NaBr declined with increasing GL concentration. The FTIR investigation hypothesized the interaction between polymer mix salt systems and added plasticizer. Infrared (FTIR) band shifts and fluctuations in intensity have been found. The ion transport characteristics such as mobility, carrier density, and diffusion were successfully calculated using the experimental impedance data that had been fitted with EEC components and dielectric parameters. CS:PVA at ambient temperature has the highest ionic conductivity of 3.8×10 S/cm for 35 wt.% of NaBr loaded with 55 wt.% of GL. The high ionic conductivity and improved transport properties revealed the suitableness of the films for energy storage device applications. The dielectric constant and dielectric loss were higher at lower frequencies. The relaxation nature of the samples was investigated using loss tangent and electric modulus plots. The peak detected in the spectra of tanδ and M″ plots and the distribution of data points are asymmetric besides the peak positions. The movements of ions are not free from the polymer chain dynamics due to viscoelastic relaxation being dominant. The distorted arcs in the Argand plot have confirmed the viscoelastic relaxation in all the prepared films.

Keywords: polymer blend electrolytes; NaBr salt; glycerol plasticizer; XRD and FTIR methods; circuit design; ion transport parameters; dielectric properties

Citation: Sadiq, N.M.; Aziz, S.B.; Kadir, M.F.Z. Development of Flexible Plasticized Ion Conducting Polymer Blend Electrolytes Based on Polyvinyl Alcohol (PVA): Chitosan (CS) with High Ion Transport Parameters Close to Gel Based Electrolytes. *Gels* **2022**, *8*, 153. https://doi.org/10.3390/gels8030153

Academic Editors: Wei Ji and Hiroyuki Takeno

Received: 25 January 2022
Accepted: 24 February 2022
Published: 2 March 2022

1. Introduction

Renewable energy sources are those derived from naturally replenishing sources, including the sun, wind, storms, seas, seeds, algae, geothermal, and biodegradable polymer materials, and they have attracted great interest due to the growing oil crisis and environmental concerns [1,2]. Polymer electrolyte (PE) science encompasses a wide range of disciplines such as polymer science, organic chemistry, electrochemistry, and inorganic chemistry [3]. Polymers are a prominent issue in material science lately, particularly solid state solutions, which are an example of ion conducting polymers [4]. Because they are

important in energy storage devices, including fuel cells, hybrid power sources, supercapacitors, and batteries, solid PEs (SPEs) have been attracting a lot of recent support [5–8]. Polar polymers can coordinate with the cations in the salt, causing it to dissolve. This is due to the presence of functional groups with high electronegativity [9]. To keep pace with rapid technological change, a new generation of highly efficient energy sources must be developed. Because of its use as an electrolyte, polymer-based ion conducting materials have sparked large interest in lithium batteries. Super-ionic conductors are solid substances in which charged atoms, known as ions, carry electric current [10]. These materials' electrical conductivity is vastly different from that of conventional semiconductors. This is because the conductivity of semiconductors is determined by the mobility of light electrons. The conductivity of super-ionic conductors, on the other hand, is the result of ion mobility. Ions have a significant amount of mass and volume [11]. As a result, electric charge transport is linked to mass transfer in super-ionic conductors [10,11].

Chitin is the world's second most abundant biopolymer, derived from fungus and insect cell walls, as well as crustacean exoskeletons [12]. Chitosan (CS), a biopolymer derived from chitin and used in a variety of medicinal and electrochemical devices, is safe, nontoxic, and biodegradable [13]. The backbone structure of CS differs from other biopolymers because it contains amino and hydroxyl functional groups [14]. Poly (vinyl alcohol) (PVA), on the other hand, is a water-soluble polymeric substance with high dielectric strength, strong charge storage capacity, and fascinating optical features [15]. In fact, the PVA molecule has a hydrophobic chain and a hydrophilic end group, the hydrophobic chains occupy space at the solid-liquid interface, while the hydrophilic end groups are extended in the outer aqueous phase. Thus, the steric hindrance and increase in the energy barrier would prevent the aggregation of the crystallinity [16]. The existence of polar groups with a high electron affinity in polar polymers is adequate to form coordination with the cation or surface groups of the fillers, resulting in a uniform nanocomposite [9,17]. PVA has a carbon chain backbone with hydroxyl groups attached, which can help build polymer composites by facilitating hydrogen bonding. Because of its high transparency and ability to form an oxygen barrier, this polymer is a suitable option for use in multilayer coatings for organic solar cells [18].

Ionic conductivity, dimensional stability, and mechanical stability are some of the latest economic and commercialization challenges in membrane technology research. Crystallinity and low ionic conductivity are two of the most significant drawbacks of SPEs [19]. Chemists and engineers are interested in the ionic conductivity of PEs since it is used in commercial electrochemical devices [20]. Both crystalline and amorphous phases exist in PEs. Polymers utilized as host materials in PEs are commonly semi-crystalline, despite the fact that ion transport occurs more frequently in amorphous rather than crystalline phases, as has long been recognized [21]. To overcome the drawbacks of SPEs and enhance conductivity, polymer blending and plasticizer addition are employed to improve ambient ionic conductivity. PVA and CS-based polymer blend complexes are simple to manufacture because of their well-controlled chemical and physical characteristics, such as toughness, homogeneity, and heat stability [22]. Blending CS and PVA is possible since they are both miscible [22]. A result of this interaction is that hydroxyl and amine groups in PVA and CS combine to form an ionic compound. For example, there are many previous works which enhance ionic conductivity by blending CS and PVA [22–25]. An XRD diffractogram revealed that the most amorphous blend host was a 50/50 mix of PVA and CS. Plasticizers may increase SPE's DC electrical conductivity by dissociating PE ion aggregates and boosting the PE's amorphous content [26].

GL, a colorless and odorless liquid, is widely available as an unavoidable by-product of the transesterification of vegetable oils used to make biodiesel, and it can also be obtained from more sustainable sources such as microalgae or cellulose. Because of its inexpensive cost, low toxicity, and unique physicochemical features, such as water solubility and hygroscopicity, it is commonly utilized in pharmaceutical formulations [27]. Increased biopolymer electrical conductivity may be achieved with the use of GL, a plasticizer rich in

hydroxyl groups, which reduces the number of internal hydrogen connections between polymer chains. This opens up new applications, such as solid PE films. Electrochemical applications such as humidity sensors, rechargeable batteries, and fuel cells might benefit from this feature's potential [28,29].

It is widespread to use dielectric relaxation spectroscopy to learn relaxation processes in complex systems from a basic perspective. Studying the dielectric characteristics of ion conducting polymers may help researchers understand more about ionic and molecular interactions. The nature of additives and temperature have a huge effect on the dielectric characteristics of ion conducting polymers [30]. The nature of charge transport in polymers has been investigated in order to better understand how these materials conduct electricity [31]. AC impedance spectroscopy is a method to look at the electrical and dielectric properties of materials. The goal of this research is to create a novel type of PE system based on a 50 percent PVA and 50 percent CS (1:1) blend that will act as a good polymer host. This study will look at the structural (XRD and FTIR), conductivity, and relaxation processes that make ions move. Particular attention is given to the exploration of the ion's relaxation and movement in the PVA:CS-based ion conducting mix electrolyte membranes. Polymer films with high content of plasticizer will offer DC conductivities close sufficient to gel-like electrolytes. Because most polymer membranes with ions that are used in devices have a high conductivity, the system made in this study could be used as an electrolyte and separator for electrochemical device applications.

2. Results and Discussion

2.1. FTIR Study

The FTIR spectroscopy is used to investigate the chemical structure of the composite films and probable interactions between the functional groups of PVA and CS in PVA:CS polymer bleed films. Additionally, in this technique, the interaction of NaBr salt with the blended PVA:CS host polymer by modifying the location, intensity, and shape of the IR transmittance bands in the wavenumber range from 500 to 4000 cm^{-1} is explored. The vibrational peaks of OH, C–O, C–H, CH_2, and C=O are used to identify the distinctive bands of PVA and CS polymers [32]. Blend polymer compatibility is shown by changes in the vibrational frequency of the peaks and improved amorphous phase in the PVA:CS system. Figure 1 shows the FTIR spectra of pure CS, PVA, and their blends. In Table 1, the FTIR peaks and their assignments are listed for pure polymers. Figure 1 shows that the OH bands in the PVA:CS system grow in size with decreased intensity, which indicates a reduction in PVA crystallinity. This is evident for the occurrence of complexation between the functional groups of the two polymers, which is clearly related to the OH band of the blend system [33]. The results of the XRD investigation are consistent with this discovery. By shifting the O–H peak position and intensity, the PVA hydrogen atoms and the CS oxygen atom are shown to establish hydrogen bonds with one other. Blending CS with PVA results in an expansion of the crystalline peak that corresponds to the C–O stretching mode and a decrease in its intensity [34]. It has been shown that adding CS to a mix diminishes the absorption band intensity at 834 cm^{-1}, which corresponds to PVA's C–C stretching.

Figure 2 illustrates the FTIR spectra of various PVA : CS : NaBr : Gl in the wavenumber range 500–4000 cm^{-1}. [35] All samples show the key characteristic absorption peaks of CS, for instance the vibration of the amino group (NH_2), O=C–NHR, and amine NH symmetric. The PVA structure has been connected to C–O plane bending, which commonly occurs at 1015–1031 cm^{-1}. Furthermore, the peak at 1600–1700 cm^{-1} is due to C=O stretching of PVA's acetate group, which is pushed to a lower wavenumber in doped samples [35].

There is motionless a noteworthy wide band at 3300–3500 cm^{-1}, despite the possibility of overlap between the N–H and O–H stretching vibrations. Figure 2 shows that as the plasticizer is increased, the bands become more intense and the wavenumber decreases. In the bands of amine (NH2) and (O–H) groups, there is a trend towards lower wavenumbers, as seen in Table 2. This strongly suggests that complexation is happened between the

electrolyte's constituents [23,36]. The shift and reduction in relative strength of these bands is due to the electrostatic interaction between the ions and the functional groups of the CS:PVA polymer blend [37]. Furthermore, the N–H stretching vibration's shift to lower wavenumbers shows that CS's intermolecular and intramolecular hydrogen bonds have decreased [38]. Recent research has shown that the carboxyl (–C=O), hydroxyl (–OH), and amine (–NH) groups all have a role in salt interaction [39]. This band's shifting and changing strength specify a superior interaction between the electrolyte's blended host polymer, salt, and plasticizer. The vibrational and stretching modes in the FTIR spectra vary as a consequence of the interaction between the electrolyte components (shown in the table below) [22,40]. This enhanced interaction promotes ion dissociation, which is beneficial to the electrolytes' ionic conductivity [40,41]. The rise in ionic conductivity is corroborated by this increase in intensity (see Figure 2).

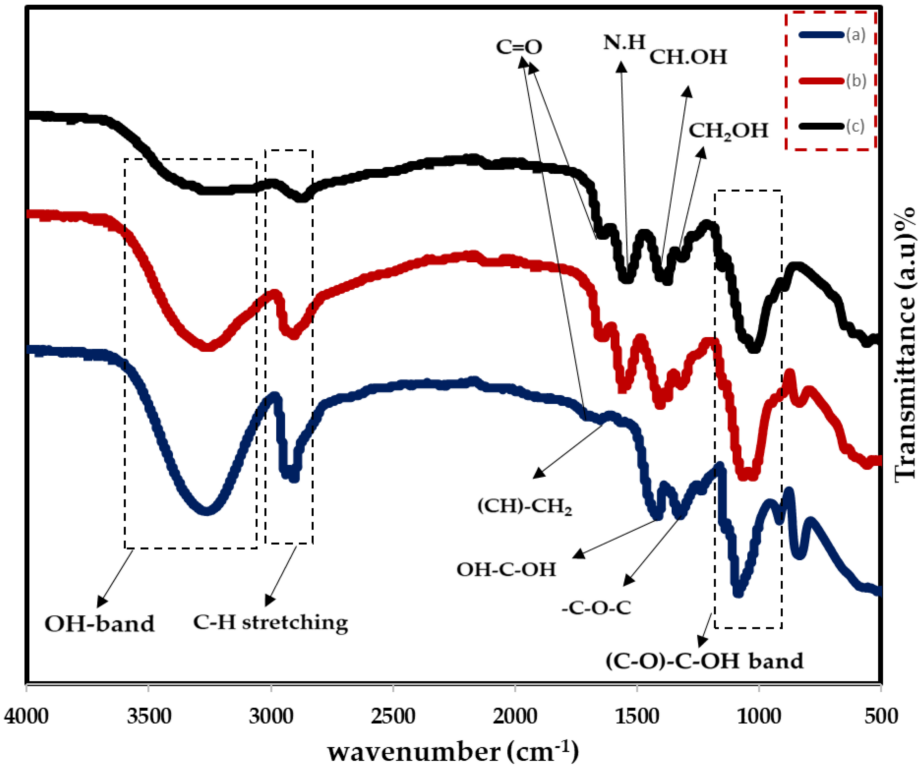

Figure 1. FTIR spectra for (**a**) pure PVA, (**b**) PVA:CS (0.5:0.5) blend, (**c**) pure CS.

Table 1. Purified (PVA), pure (CS) and blended pure (PVA:CS) FTIR data are shown.

Vibrational Modes	Pure PVA	Vibrational Modes	PVA:CS	Vibrational Modes	Pure CS
O–H stretching	3259.34	O–H stretching	3261.67	O–H stretching	3261.42
C–H stretching	2937.98	C–H stretching	2906.38	C–H stretching	2872.47
C = O	1710	C = O	1646.29	C = O	1636.33
(C–H)–CH2	1653.51	N–H	1557.41	N–H	1540.59
OH–C–OH	1417.33	CH·OH	1405.89	CH·OH	1403.24
–C–O–C	1324.90	CH2–OH	1376.61	CH2–OH	1375.46
(C–O)–C–OH	1084.88	(C–O)–C–OH	1027.48	(C–O)–C–OH	1022.98
C–C	834.16	C–C	834.08	C–C	–

2.2. XRD Study

Figure 3 shows XRD results for room-temperature PVA, CS, and CS:PVA (a–c). In contrast to the semi-crystalline character of pure PVA (Figure 3a), the CS exhibits crystallinity maxima at some 2θdegree values (Figure 3b) [42]. Since OH groups are present everywhere throughout PVA and CS's main chain, it is able to form strong inter- and intramolecular

hydrogen bonds. Amorphous phases in PVA are responsible for the large peak at 2θ = 40.7° which is due to existing high water content [43]. The XRD pattern of CS: PVA (Figure 3c) revealed two hallows and smaller crystalline peaks in the current study. It is worth noting that, as the vast hallows demonstrate, CS: PVA is less crystalline than pure PVA or CS alone, and its structure is practically amorphous [44,45]. According to previous research, the amorphous structure of PEs is linked to large diffraction peaks [46].

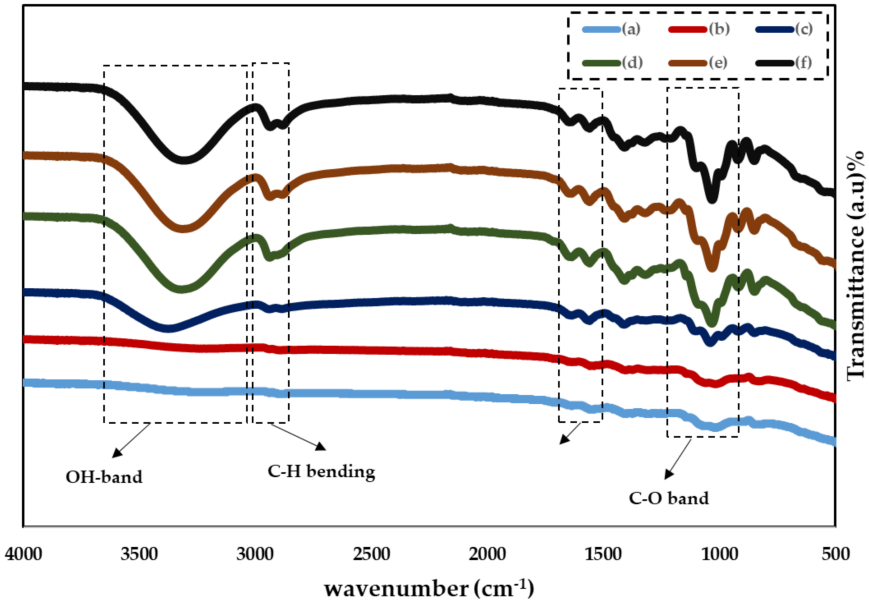

Figure 2. FTIR spectra of (**a**)CSPVNG0, (**b**) CSPVNG11, (**c**) CSPVNG22, (**d**) CSPVNG33, (**e**) CSPVNG44 and (**f**) CSPVNG55.

Table 2. Assignments of FTIR bands for PVA:CS: NaBr:GL solid PEs.

Samples	Wavenumbers (cm^{-1})			
	C–O Band	NH_2	C–H Band	O–H Band
CSPVNG0	1015.61	1545.66	-	-
CSPVNG11	1020.04	1558.79	-	3374.36
CSPVNG22	1039.06	1559.40	2938.77	3374.69
CSPVNG33	1032.10	1559.33	2938.70	3317.19
CSPVNG44	1031.21	1559.41	2937.25	3316.19
CSPVNG55	1031.29	1559.47	2936.4	3312.77

Meanwhile, when GL was added to these samples, the strength of the CS : PVA : NaBr peaks decreased, and the wide nature of the peaks improved, as seen in Figure 4a–f. These findings support the hypothesis that the PE has an amorphous structure that improves conductivity by increasing ionic diffusivity. Furthermore, the NaBr salt dissociates completely in the PE, leaving no peak associated with pure NaBr, as illustrated in Figure 5. The absence of hydrogen bonds between polymer chains is a likely cause for the intensity drop and broadening, indicating the presence of the amorphous phase in the samples [47]. Plasticized PEs are a type of PE made by adding low molecular weight chemicals to the polymer host, such as ethylene carbonate, propylene carbonate, and poly ethylene glycol (PEG) [48]. It is possible for plasticizers to reduce the number of active centers in polymer chains, hence decreasing the interactions between and within molecules [49]. Consequently, the three-dimensional structure generated during drying loses stiffness and the mechanical and thermomechanical characteristics of the films it produces are affected [49,50]. To facilitate charge carrier transfer, low molecular weight plasticizers have been added, resulting in a reduction in crystallinity, an increase in salt dissociation capacity and producing a jelly thin film, as seen in Figure 6a,b.

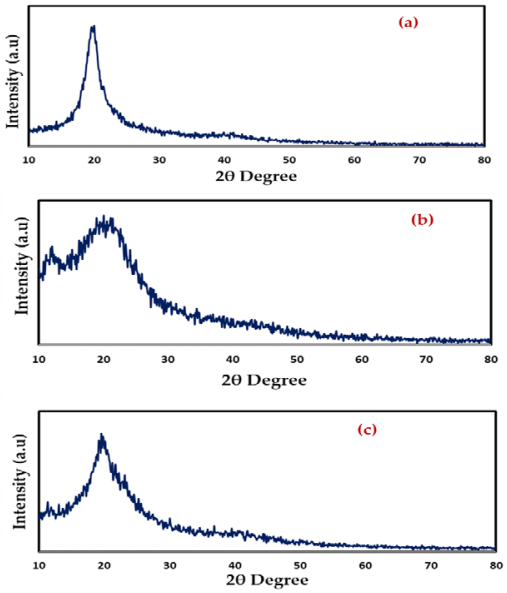

Figure 3. XRD pattern of (**a**) pure PVA film, (**b**) pure CS and (**c**) PVA: CS blend (50:50) films.

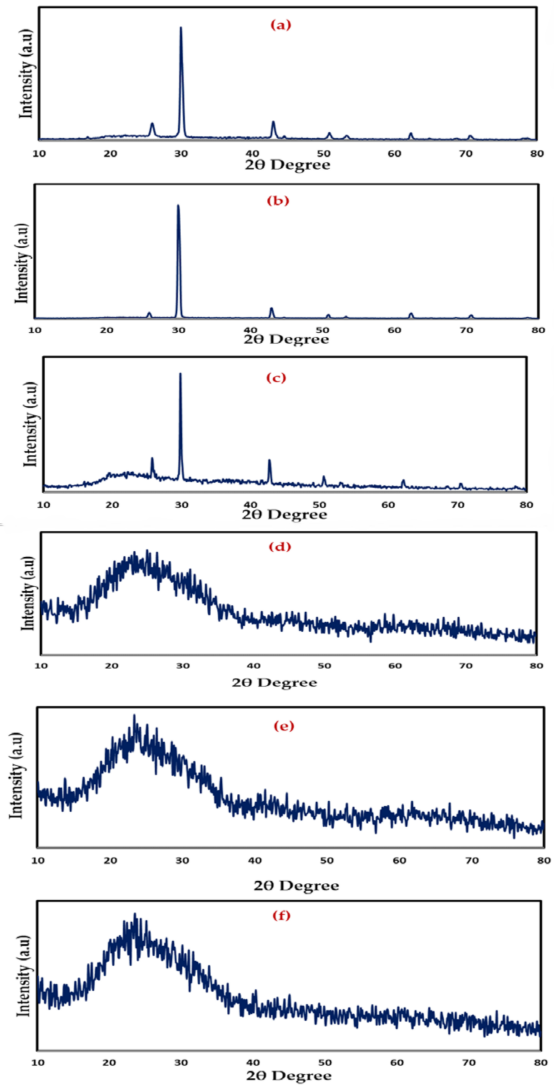

Figure 4. XRD Pattern of (**a**) CSPVNG0, (**b**) CSPVNG11, (**c**) CSPVNG22, (**d**) CSPVNG33, (**e**) CSPVNG44 and (**f**) CSPVNG55.

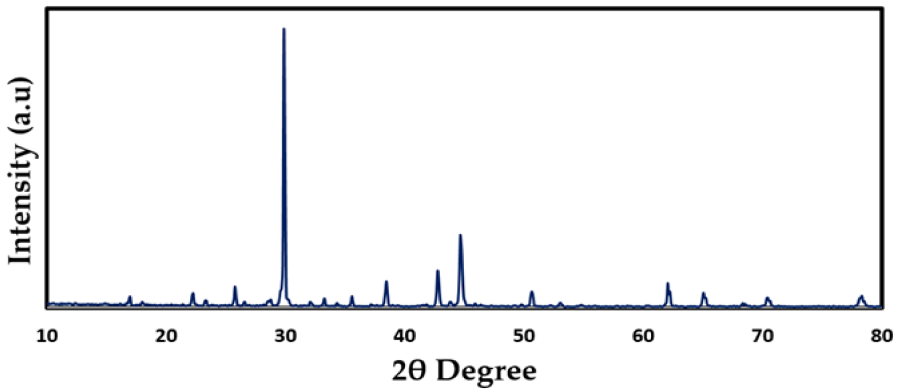

Figure 5. XRD pattern of pure NaBr.

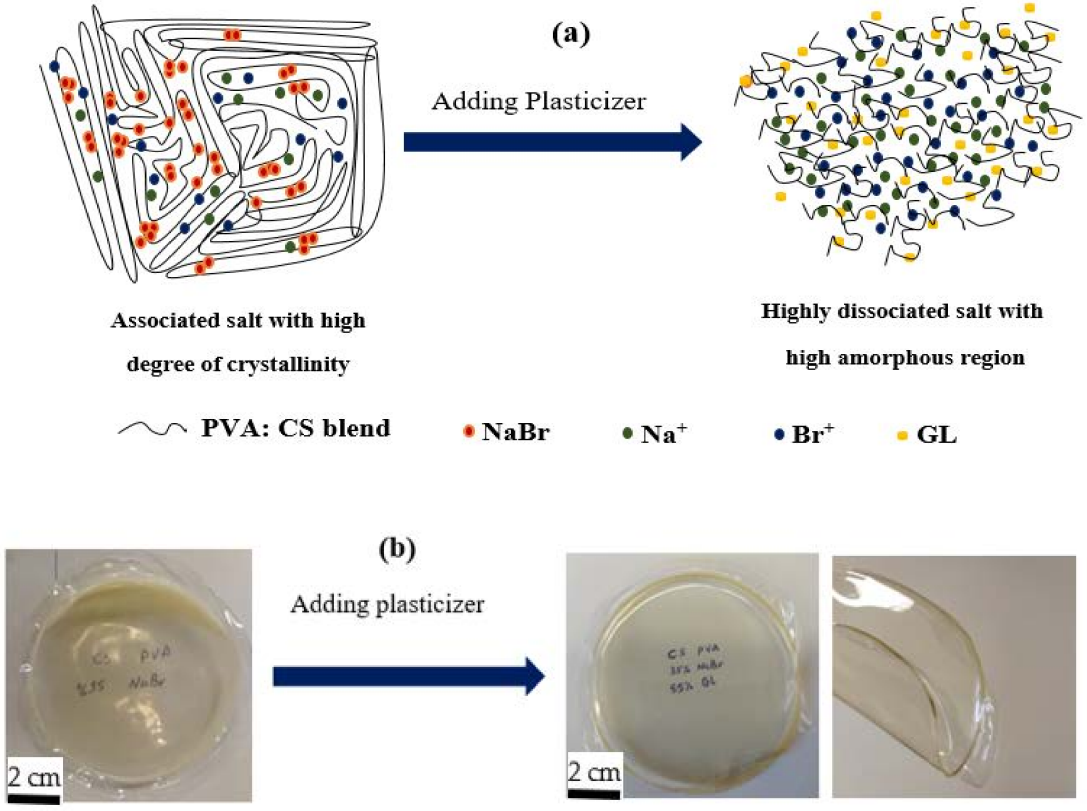

Figure 6. Role of plasticizer on (**a**) the ion dissociation and increase of flexibility and amorphous phase, and (**b**) the film with high content of plasticizer can easily be bending without deformation or tear. The last photograph shows the ability of the film to bending.

2.3. Complex Impedance Spectroscopy (CIS) and Ion Transport Study

It is required to conduct non-destructive testing in order to distinguish a wide range of materials. As a tool for studying heterogeneous systems, dielectric impedance spectroscopy, which measures conductivity and permittivity as a function of frequency at different temperatures, may reveal their structure [51]. The CIS response is seen in the Nyquist plot of all the samples, as shown in Figure 7a–e. In the high frequency and low frequency regions, the responses take the shape of a semicircle and a tail (spike), respectively. On the one hand, at high frequencies, the incomplete semicircle is primarily associated with bulk resistance (a bulk property). The development of a spike, on the other hand, denotes the establishment of double layer capacitance at the electrode/sample interface at low frequencies [52].

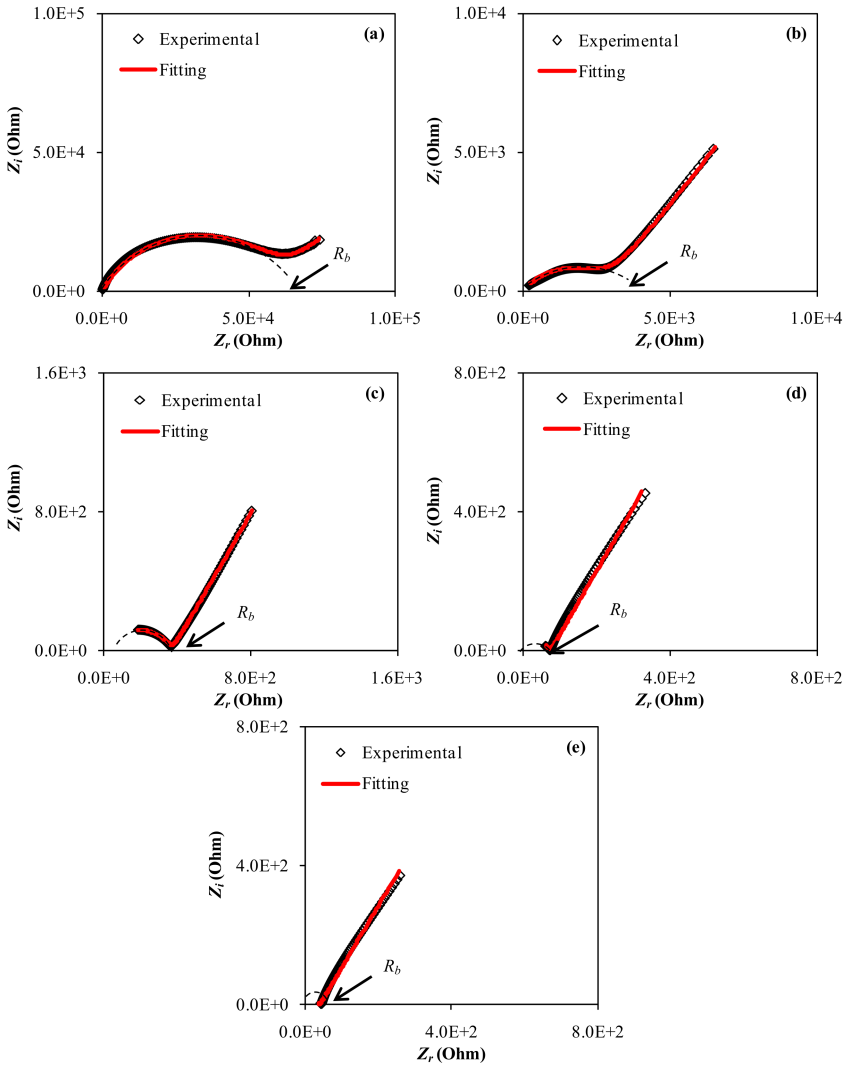

Figure 7. EIS plots for (**a**) CSPVNG11, (**b**) CSPVNG22, (**c**) CSPVNG33, (**d**) CSPVNG44 and (**e**) CSPVNG55 electrolyte films.

The facility to recognize the relaxation frequency and to separate electrode (low frequency spike) and bulk (high frequency semicircular region) affects are two of the benefits of the CIS technique. Real (Z′) and imaginary (Z′′) components of impedance can be obtained using the CIS approach across a large frequency range. This technique has been effectively utilized to assess DC ionic conductivity and ionic conductor activation energy in recent years [44,53]. An electrochemical sample holder must be exposed to an alternating voltage across a wide frequency range for CIS measurements [54]. The direct correlation between the system's response and the proposed equivalent circuit, which represents the system's electrical behavior, is a key element of CIS [55,56]. In physics, a dielectric material's dissipative response is characterized by a resistance (R), whereas its storing response is characterized by a capacitance (C) [56,57]. One of the outputs of electrical impedance spectroscopy is a graph of the imaginary component of the impedance vs. the real component, CIS. This graph can be used to derive information about the expected equivalent circuit. The impedance charts should have a straight line parallel to the imaginary axis at low frequencies; instead, the blocking electrode polarization effect (double layer capacitance) produces the curvature [58–60].

It will be simple to specify the mechanism of the system after fitting experimental spectra and analyzing using the electrical equivalent circuit (EEC) technique [59]. Figures 7 and 8 show the experimental impedance spectra, as well as the related EEC

models for all of the electrolyte samples. In the Nyquist plots displayed in the insets of the bulk resistance (R_b) for charge carriers in electrolyte systems, as well as two constant phase elements (CPEs); CPE1 and CPE2, can be seen Figure 8. The EEC is made up of a succession of R_b and CPE1 in parallel with a second CPE2 (from the tilted spike). The impedance's ZCPE component is written as follows [55,61,62]:

$$Z_{CPE} = \frac{1}{C\omega^{p}}\left[\cos\left(\frac{\pi p}{2}\right) - i\,\sin\left(\frac{\pi p}{2}\right)\right] \quad (1)$$

where CPE capacitance and the angular frequency are symbolized as C and ω, and represents the departure of the plot from the vertical axis in complex impedance spectra. It is important to point out that CPE and capacitor are commonly used interchangeably in the context of an EEC modeling.

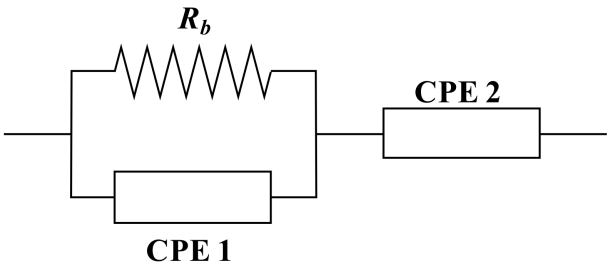

Figure 8. The equivalent electrical circuit (EEC).

The overall mathematical expression of the equivalent circuit, and the real (Z_r) and imaginary (Z_i) complex impedance (Z*) values may be written as follows [55,61,62]:

$$Z_r = \frac{N + R_b}{M + T} + \frac{\cos(\frac{\pi p_2}{2})}{C_2\omega^{p2}} \quad (2)$$

$$Z_i = \frac{L}{M + T} + \frac{\sin(\frac{\pi p_2}{2})}{C_2\omega^{p2}} \quad (3)$$

where $N = R_b^2 C_1 \omega^{p1} \cos\left(\frac{\pi p_1}{2}\right)$, $M = 2R_b C_1 \omega^{p} \cos(\frac{\pi p}{2})$, $L = R_b^2 C_1 \omega^{p1} \sin\left(\frac{\pi p_1}{2}\right)$ and $T = R_b^2 C_1^2 \omega^{2p} + 1$.

The real and imaginary sections of semicircles are attributed to the first half of Equations (8) and (9), while spike lines are attributed to the second part. Where C_1 indicates CPE1's bulk capacitance and C_2 denotes CPE2's capacitance at the electrode-electrolyte interface. In Table 3, the EEC fitting parameters are listed. In the high frequency region, the semicircle size drops significantly as the amount of GL increases, as seen in the impedance spectra. Figure 7a,b show how to model an incomplete semicircle in which the value of R_b is in series with one CPE element and parallel with another CPE element (at low frequency tail). Figure 7c–e illustrate the complete elimination of the incomplete semicircle. Given the R_b values and the film thickness, calculation of the DC conductivity can be performed using Equation (4) [63].

$$\sigma_{dc} = \left(\frac{1}{R_b}\right) \times \left(\frac{t}{A}\right) \quad (4)$$

Table 3. Circuit elements of the plasticized PBE systems.

Sample	p_1 (rad)	p_2 (rad)	CPE1 (F)	CPE2 (F)
CSPVNG11	0.71	0.52	6.67×10^{-9}	1.54×10^{-6}
CSPVNG22	0.60	0.60	1.43×10^{-7}	3.33×10^{-6}
CSPVNG33	0.73	0.68	2.22×10^{-8}	1.35×10^{-5}
CSPVNG44	0.71	0.68	5.00×10^{-8}	2.38×10^{-5}
CSPVNG55	0.64	0.67	1.00×10^{-7}	2.94×10^{-5}

Table 4 shows the computed DC conductivity and bulk resistance (R_b) values, as well as all the transport parameters of the plasticized PBE systems, including diffusion (D), mobility (μ) and charge carrier density (n). The quantity and sort of plasticizer have a big impact on the PEs' characteristics. GL is the mainly often used and least expensive plasticizer [64]. After water, it is one of the most well-known polar compounds. It is completely water soluble, has a low toxicity compared to other organic solvents, and is completely biodegradable [27]. Furthermore, renewable resources are abundant on the earth and have a low market price. The relatively high conductivity can be explained by the massive ion movement, as demonstrated by the semicircle disappearing in the high frequency area of the spectra. As a result, GL is an effective plasticizer for reducing crystallinity and increasing ion mobility, which increases overall DC conductivity. According to Kaori Kobayashi et al., the addition of GL plasticizer reduced the glass transition temperature and increased the dc conductivity (σ_{dc}) of poly (ethylene carbonate) (PEC): LiPF6Telectrolyte [65].

Table 4. Transport parameters of the plasticized PBE systems.

Sample	Rb (Ω)	σ (S cm^{-1})	D (cm^{2}s^{-1})	μ (cm^{2}V^{-1}s)	n (cm^{-3})
CSPVNG11	62,600	2.46×10^{-7}	3.48×10^{-5}	1.35×10^{-3}	1.14×10^{15}
CSPVNG22	2815	5.48×10^{-6}	1.52×10^{-5}	5.90×10^{-4}	5.79×10^{16}
CSPVNG33	369	4.18×10^{-5}	8.60×10^{-7}	3.35×10^{-5}	7.79×10^{18}
CSPVNG44	73	2.11×10^{-4}	4.06×10^{-7}	1.58×10^{-5}	8.34×10^{19}
CSPVNG55	40	3.86×10^{-4}	1.46×10^{-7}	5.67×10^{-6}	4.24×10^{20}

The heart of electrochemical devices is PEs. The majority of solid-state electrochemistry research is focused on the development of high ion-conducting materials for energy conversion and storage [66]. Massive research efforts over the past two decades have resulted in systems with enhanced conductivity and transport characteristics, and PEs fall into this category [66–68]. Transport parameters are crucial properties that should be considered in device applications. PEs with performance transport properties are the focus of many research groups.

Ion number density (n), diffusion coefficient (D), and mobility (μ) may be calculated from the impedance data of all systems by utilizing the following relations [69–71]:

$$D = \left\{ \frac{(K_2 \varepsilon_0 \varepsilon_r A)^2}{\tau_2} \right\} \quad (5)$$

where ε_r and ε_0 signify the dielectric constant and the permittivity of the space, respectively. The reciprocal of ω is represented by τ_2, which is matching to the smallest value in Z_i. From Equation (5), it is noticeable that three parameters influence the value of D, which are K_2, ε_r and τ_2. Thus, it is difficult to obtain D and μ values follow the trend of n value.

$$\mu = \left\{ \frac{eD}{K_b T} \right\} \quad (6)$$

where k_b and T refer to the Boltzmann constant and absolute temperature, respectively. DC conductivity (σ_{dc}) and Ion number density (n) are presented by the following equations, respectively:

$$\sigma_{dc} = ne\mu \quad (7)$$

$$n = \left\{ \frac{\sigma_{dc} K_b T \varepsilon \tau_2}{(eK_2 \varepsilon_0 \varepsilon_r A)^2} \right\} \quad (8)$$

From Table 4, is clear that the number density improved from 1.14×10^{15} cm^{-3} to 4.24×10^{20} cm^{-3}. A large network of ion conduction may be formed by the incorporation of plasticizer molecules into the host polymer, as shown in Figure 6a [72]. According to recent research, the conductivity of thin films may be improved by increasing the amount of existing hydroxyl groups [73]. To lower intermolecular tensions, increase the mobility

of its polymeric chains and enhance mechanical properties such as the extensibility of the resultant film, GL was essential [28,74].

2.4. Dielectric Properties

For determining the electrical characteristics of many materials, including glasses, semiconductors, polymers, and transition metal oxides, impedance spectroscopy may be a valuable instrument [9,40]. CIS relies on a number of other measured or calculated parameters. The measurement, analysis, and charting of some or all of the four impedance-related functions (Z*, Y*, M*, and ε*) in the complex plane is referred to as impedance spectroscopy [75]. Dielectric measurements (ε*), such as dielectric constant (ε') and dielectric loss (ε''), disclose a lot about polymer chemical and structural behavior. Using Equations (9) and (10), the real and imaginary parts of dielectric function were evaluated [76]. Because of the electrode polarization (EP) effect [77], both of them (ε' and ε'') are quite high at low frequencies, as seen in Figures 9 and 10. The inclusion of another polymer or a dopant in the polymer has a significant impact on these properties (ε' and ε'') [56]. In polymer electrolyte systems the polarization can be resulted from both permanent dipole of host matrix functional groups and space charge polarization at the electrode/electrolyte interface. As can be seen in Figure 10, the dielectric loss has recorded high value at low frequency region due to the plenty of time that is provided by the applied field for re-orientation. In addition, the increasing plasticizer has improved the rotation freedom of the site groups to response quickly to the applied field. These two factors have caused an enhancement in dielectric loss value. However, at high frequency regions such a high value is not observed due to the fast switching of the applied field.

$$\varepsilon' = \frac{Z_i}{\omega C_0 \left(Z_r^2 + Z_i^2\right)} \tag{9}$$

$$\varepsilon'' = \frac{Z_r}{\omega C_0 \left(Z_r^2 + Z_i^2\right)} \tag{10}$$

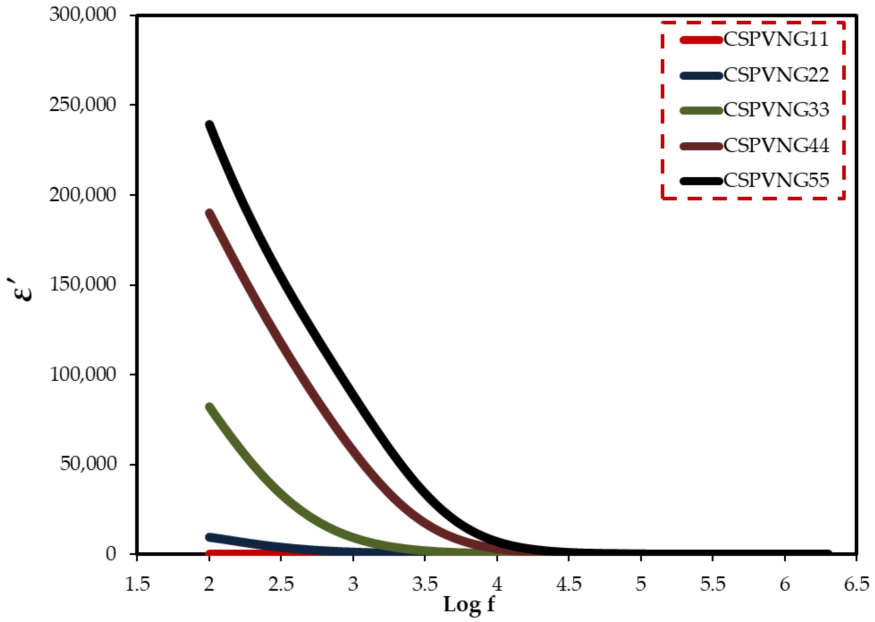

Figure 9. Dielectric constant versus log(f) for the electrolyte samples.

The vacuum capacitance, C_o, is provided by the formula $\varepsilon_o A/t$, where ε_o is the free space permittivity, which is to 8.85×10^{-12} F/m. If f is the applied field frequency, the angular frequency (ω) is equal to $2\pi f$.

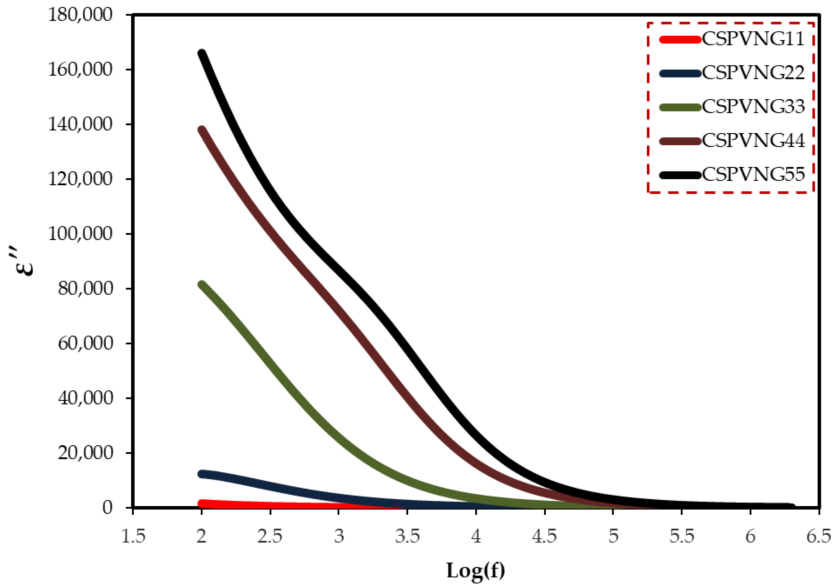

Figure 10. Dielectric loss versus log(f) for the electrolyte samples.

At low frequencies, ion migration and polarization have a significant impact on dielectric properties. For polymer/filler composites, this phenomenon is not possible. Due to the delayed dielectric relaxation of various polarizations in polymer composites, the permittivity falls gradually with increasing frequency. Permittivity has a low frequency dependency, which is advantageous across a large frequency range [78].

The migration of ions from one site to another in solid PEs will cause the electric potential of the environment to be perturbed. The perturb potential will have an impact on the movement of the other ions in this location. Non-exponential decay, or conduction processes with a dispersion of relaxation time, will occur as a result of such cooperative ion motion [79]. The behavior of bulk dielectric constant and bulk DC conductivity is essentially identical with GL content, as can be seen. This finding demonstrates that DC conductivity is greatly influenced by the dielectric constant. It is important to note that as the plasticizer concentration rises, the dielectric dispersion switches to the high frequency region. Both DC conductivity and ε' are clearly lower for Gl content of 10 to 20 Gl. When crystallites cover a significant percentage of the polymer, the conductivity and dielectric constant are dramatically reduced, which is an undesirable circumstance [80]. Most of the dielectric constant is reduced by structural densification (i.e., the rise in crystallinity between the provided lamellae). Charge carrier mobility is hindered during the remainder of the amorphous phase as a consequence. The conduction channel may become unstable even if the amorphous phase composition changes slightly in such a compact arrangement. There is also the possibility that electrode contact loss and sample stiffness are to blame for such a large conductivity decline or resistivity rise [81]. Usually, the dominance of the EP effect can be attributed to significant charge carrier buildup at high GL concentration or at high temperature at the electrode/electrolyte interface because at these situations the semicircle disappears in CIS plots [82].

When an electric field is given to a solid substance, it causes ion conduction between favorable binding sites. The tail at low frequencies may be owing to the electrode/electrolyte interfaces blocking mobile ions and/or equipment constraints in viewing the low-frequency electrode polarization region [83]. The magnitude of ionic conductivity is described in theory as

$$\sigma = \sum q_i n_i \mu_i \quad (11)$$

where n_i denotes the number of carriers, and q_i and μ_i denote the carriers' charge and mobility, respectively. To achieve good ionic conductivity, you will need a lot of ion carriers with a large mobility. As a result, it is critical to discover materials that match these require-

ments [84]. The concentration of charge carriers' growths when the dielectric constant rises $\left(n_i = n_o \exp\left(-\frac{U}{\varepsilon' K_B T}\right)\right)$, where U denotes the dissociation energy, resulting in anincrease in DC conductivity $(\sigma = \sum q_i n_i \mu_i)$.

2.5. Tanδ Study

Broadband dielectric spectroscopy has been revealed to be a very efficient method for studying polymeric system relaxation processes. The complex dielectric utility, ε*, which consists of the dielectric constant and loss, is a material parameter that is affected by frequency, temperature, and structure, and so the tan, which is the ratio of ε'' to ε', is likewise frequency dependent. The plot of tanδ dielectric relaxation peaks as a function of frequency at room temperature for all samples is explored in this section. The aim of this study is to learn more about the relaxation processes and structure of polymeric-based materials. The study of dielectric relaxation can be a useful technique for understanding dipole relaxation in PEs. The dielectric relaxation processes are usually linked to one or more of the material's polarization processes. The dipolar polarization and polarization owing to migrating charges are the two major components of polymer dielectric response. In frequencies less than 10^9 Hz, dipolar and migrating charge polarizations can be identified [85]. To our understanding, there is no literature that discusses the use of loss tangent (Tanδ) relaxation peaks in determining polymeric structural attributes. The mechanism of ion transport is presently under debate among scientists. As a result, the study's primary contribution is to provide the first experimental data and insights into the tan relaxation peaks and structure identification. The dielectric loss peak has been recognized as useful in investigating relaxations such as, α, β and γ, which are connected to dipole rotation in the crystalline phase, dipole orientation in amorphous areas, and side group or end-group movement in the amorphous phase, respectively [86]. α relaxation occurs at low frequencies most of the time, but β relaxation can be seen at intermediate to higher frequencies, and it transitions to higher frequencies as the amorphous phases increases [55]. The height of the peak associated with the amorphous phase at high frequency is clearly increased as the GL content increases. The results of the morphological and impedance analyses are exactly in line with these conclusions. As a result, the loss tangent peak can be used to determine structural features of materials in a sensitive manner. PEs are known to be heterogeneous materials, as both amorphous and crystalline phases exist. At high GL concentrations, the single peak disappears, implying system homogeneity [87]. The findings in this work suggest that tanδ relaxation peaks can be used to distinguish between crystalline and amorphous polymer phases. Furthermore, one peak formed at 10 wt.% of GL, while two loss peaks appeared at 20 wt.% of GL, as shown in Figure 11a. In both crystalline and amorphous regions, the peaks are connected to dipole orientation. The α -relaxation loss peak was discovered to be narrower and asymmetrical than the β -relaxation peak. The α -relaxation is partially filtered at low frequencies due to ionic conductivity [55,88]. While Figure 11b shows that α -relaxation loss peak has been disappeared, and β -relaxation peak has dominated due to the transfer of these systems from crystalline phase to fully amorphous phase, which is supported by XRD results (Figure 4).

2.6. Electric Modulus and Relaxation Study

The material is exposed to an alternating electric field, which is generated by applying a sinusoidal voltage, in dielectric measurements; this process causes dipoles in the material to align, resulting in polarization. Dipoles on the side chain of the polymer backbone can cause dipolar polarization in polymeric materials, as well as the presence of ion translational diffusion [89]. Because of the huge conductivity effects, dielectric parameters should be expressed in terms of the complex electric modulus ($M^* = 1/\varepsilon^*$) [90]. It can be deduced from the electric modulus study that ion transport happens either by polymer segmental relaxation or conductivity relaxation [91]. Electrical relaxation phenomena in PE are known to be caused by phase transitions, interfacial effects, and polarization or conductivity

mechanisms [92]. Macedo et al. devised the electric modulus formalism to limit the effect of electrode polarization. Equations (12) and (13) were used to compute the real and imaginary components of electric modulus [93]. The peak maximum in the imaginary part of the electric modulus indicates that the sample is an ion conductor. Figure 12 depicts the frequency dependence of M′ for various GL plasticizer concentrations. Figure 13 shows that a distinct relaxation peak can be detected in the imaginary part of modulus (M′′) spectra, which is associated with conductivity processes, however no peak can be found in the dielectric loss spectra. This indicates that ionic and polymer segmental movements are highly connected, as evidenced by a single peak in the M′′ spectra and no equivalent characteristic in dielectric loss spectra (Figure 13) [94]. As a result, charge migration of ions between coordinated sites of the polymer and segmental relaxation of the polymer are both involved in conduction in PEs.

$$M' = \omega C_0 Z_i \quad (12)$$

$$M'' = \omega C_0 Z_r \quad (13)$$

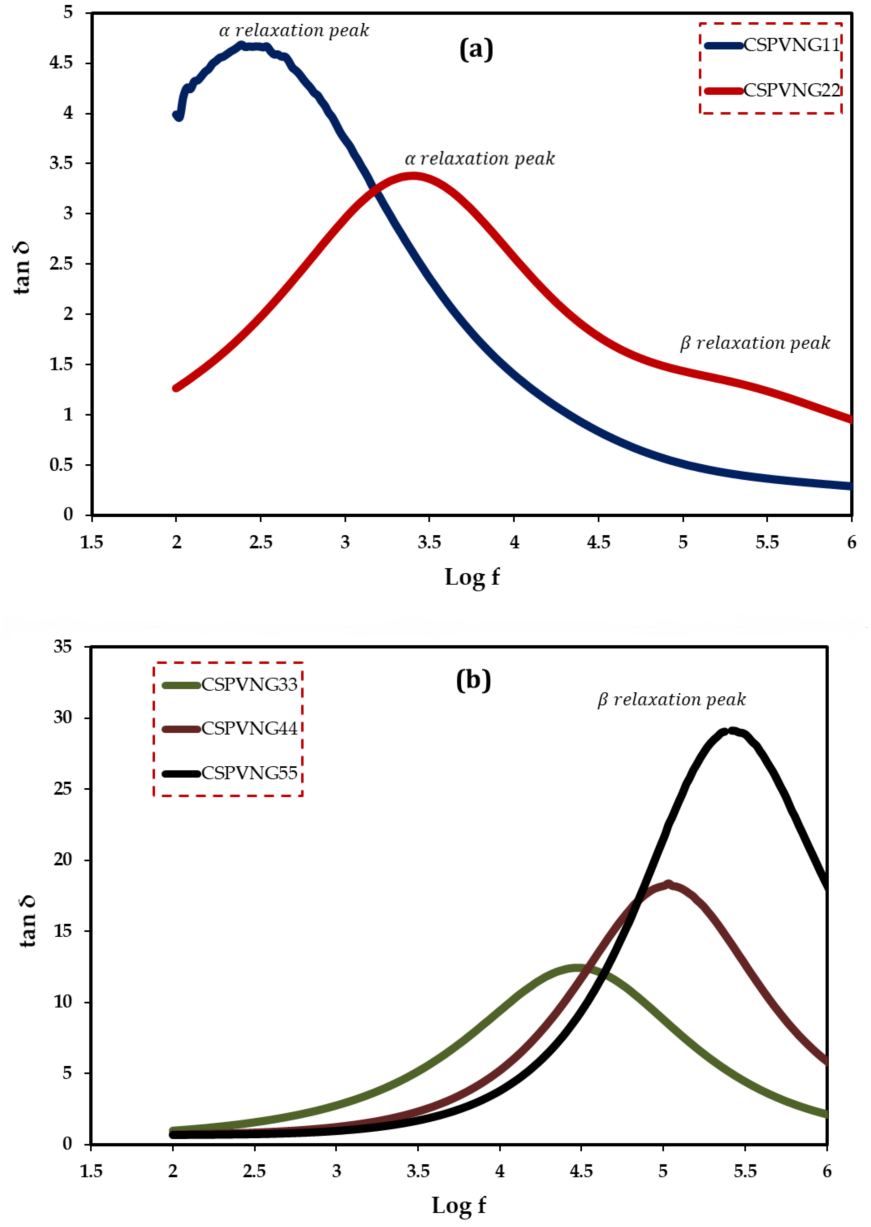

Figure 11. Loss tangent versus log (f) for (**a**) CSPVNG11 and CSPVNG12, and (**b**) CSPVNG33, CSPVNG44 and CSPVNG55 the electrolyte samples.

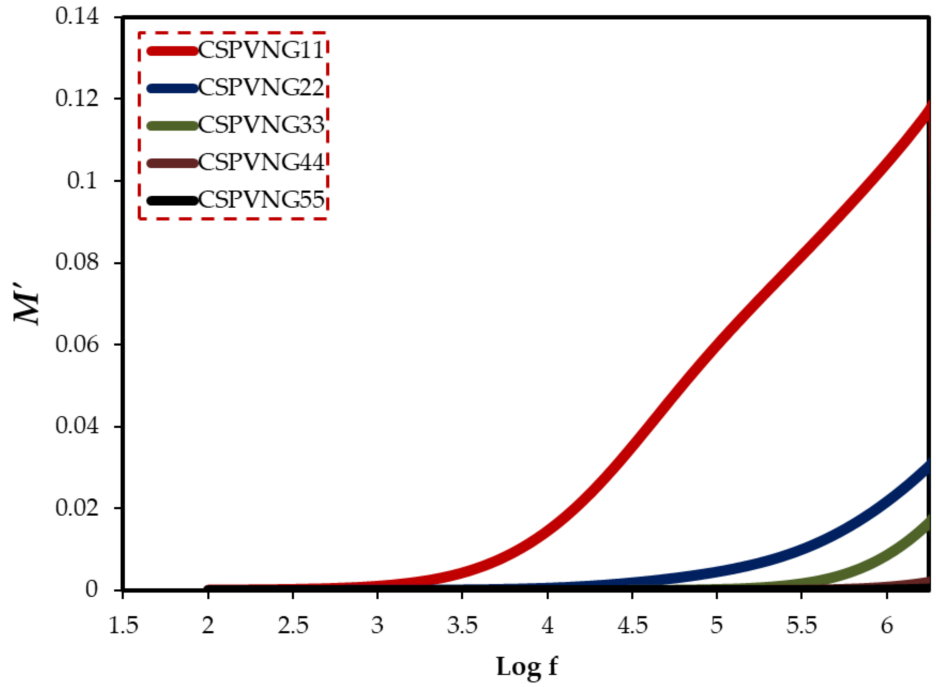

Figure 12. The real part of the electric modulus versus log (f) for the electrolyte samples.

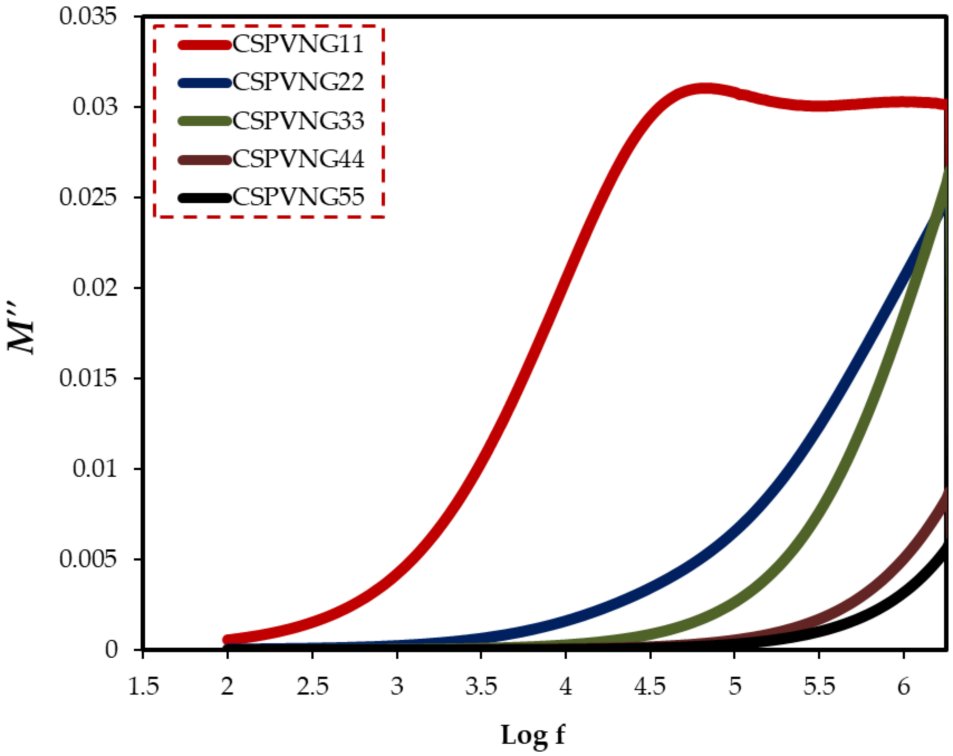

Figure 13. The imaginary part of the electric modulus versus log (f) for all electrolyte samples.

The use of Argand (M″ vs. M′) plots to decide whether a relaxation dynamic fits in to viscoelastic or conductivity relaxation is a well-known approach. The type of relaxation processes in the current PEs can be revealed. The Argand curves for all of the samples are shown in Figure 14 at room temperature. According to [95], if the Argand plot between the imaginary component (M″) and the real part (M′) of the electric modulus displays semicircular behavior, the relaxation is due to conductivity relaxation; otherwise, viscoelastic relaxation (or polymer molecular relaxation) is responsible [96]. The circle

diameters do not line up with the real axis. This means that ion transport happens in all samples via viscoelastic relaxation. The conductivity relaxation differs significantly from the viscoelastic relaxations found in polymers. The conductivity relaxation corresponds to a single-relaxation-time Debye model process, whereas viscoelastic relaxations are known to have a dispersion of relaxation times [97].

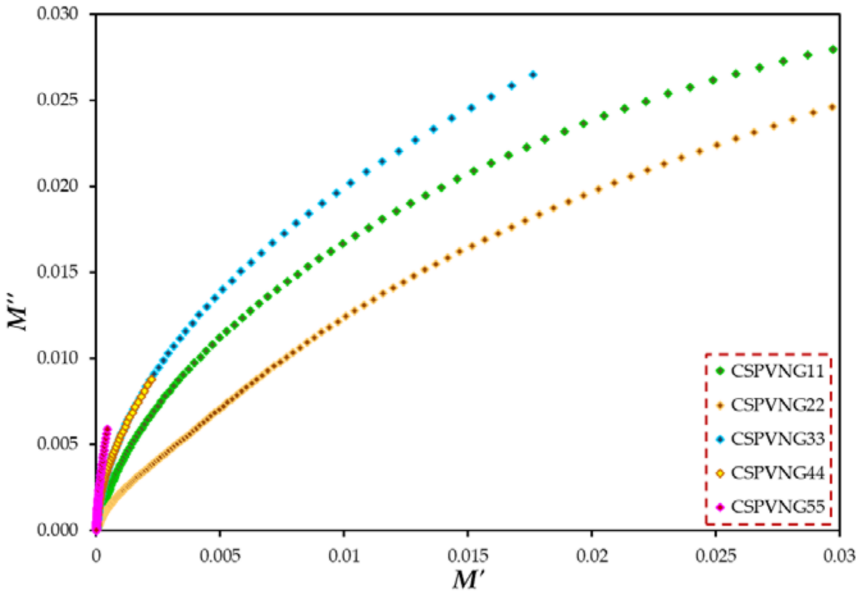

Figure 14. M′′-M′ plot for all plasticized SPE films.

2.7. AC Conductivity Analysis (σ_{ac})

Even though experiments have been carried out on a broad range of semiconducting and insulating materials, the literature on AC conductivity in disorder solids and its characteristics with composition is valuable. In general, frequency-dependent conductivity follows a power-law behavior ($\sigma \sim \omega^s$) [98]. The properties of crystalline semiconductors and insulators have been determined by several solid state theories, but when these theories are applied to data on polymers, the predictions they produce are not sufficiently unique, making it surprisingly difficult to determine all the important characteristics of electrical conduction in polymers even today [99]. The σ_{ac} were evaluated from the real (Z_r) and imaginary (Z_i) parts of complex impedance (Z^*) using Equation (14).

$$\sigma'_{ac} = \left[\frac{Z_r}{Z_r^2 + Z_i^2}\right] \times \left(\frac{t}{A}\right) \quad (14)$$

Figure 15 shows the AC conductivity spectra of plasticized PVA : CS : NaBr sheets at ambient temperatures. At high frequencies, ac conductivity in disordered solids is highly dispersed, making it one of the most distinctive properties of electrical conduction in these materials. AC methods are widely used to study electrical properties of ionically conducting materials, which would need the construction of non-blocking electrodes for DC research [100]. Frequency dependent data may be used to highlight the contributions of bulk materials (high frequency semicircle area), grain boundaries, and electrode-electrolyte effects (low frequency spike region) [101]. In the GL range of 11 to 33 wt.%, the ac conductivity spectra (see Figure 15) may be separated into three discrete regions. The electrode-electrolyte interfacial phenomenon known as electrode polarization (EP) effect caused the low frequency area (region I) to appear as a spike [102]. It is worth noting that a linear relation between the spike region and GL content can be observed. A plateau of ac conductivity is identified in the intermediate frequency band (region II), which correlates to DC conductivity. As a result of increased electrode polarization (EP) and a shift to the higher frequency side, this region (plateau region) grows dramatically

with increasing GL content. At high GL concentrations, the disappearance of the high frequency semicircle in the impedance plot (Z_i-Z_r) is closely related to the lowering of dispersion region (Figure 7a–e). These dispersion areas are critical for determining the ion conduction type in solid PEs.

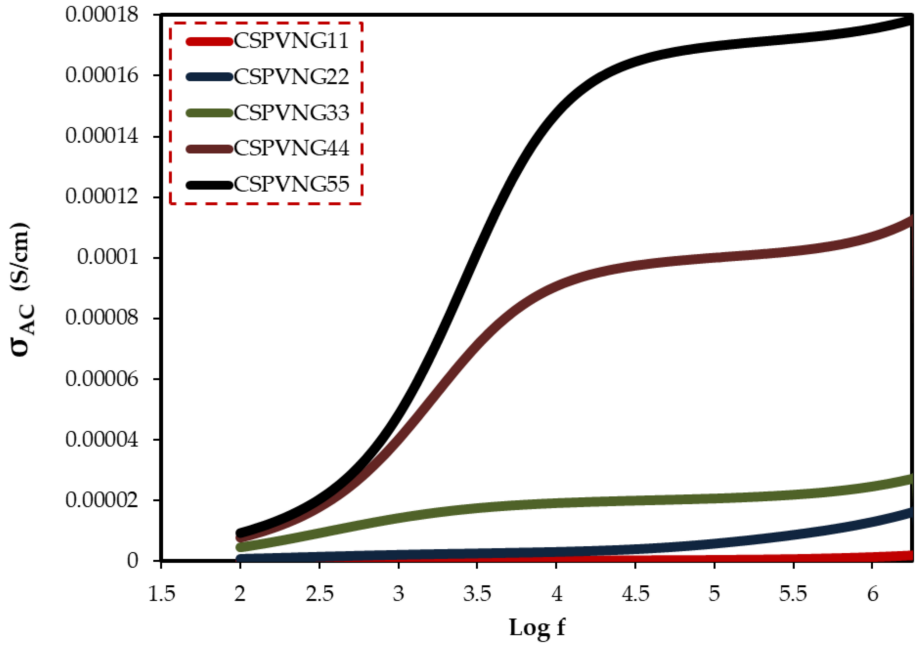

Figure 15. AC conductivity spectra.

The Jonscher's relation is a good way to describe the link between ac conductivity and charge carrier motion [103]:

$$\sigma_{dc}(\omega) = \sigma_{dc} + A\omega^s \ (0 < s < 1) \quad (15)$$

where σ_{dc} denotes the frequency-independent dc conductivity, A denotes a temperature-dependent constant, and s denotes the charge carrier interactions during hopping processes [104]. The second component is caused by accumulated interfacial charges and permanent/induced polarization (restricted mobility) of the dipoles. As frequency rises, the total conductivity of the second component due to polarization increases, according to Equation (15) [105]. $\sigma'_{ac}(\omega)$ represents the charge transport mechanism and many-body interactions among charge carriers [104,106].

3. Conclusions

Finally, the casting approach was employed to make plasticized PBEs based on polyvinyl alcohol (PVA): chitosan (CS) polymers. The samples structural and electrical properties were investigated using a variety of techniques including XRD, FTIR and EIS. There is interaction at the molecular level, as shown by shifting peaks and changes in the intensity of FTIR bands. PVA and CS polymers behave semicrystallinly, as shown by the XRD data. It was determined that the samples inserted with high content of GL were amorphous due to the XRD pattern exhibiting a wide hum. The GL plasticizer fastened the dissociation of NaBr salt and reduced the crystallinity of polymers. For a sample containing 55 wt% GL, the CIS approach revealed a maximum ionic conductivity of 3.8×10^{-4} S/cm. Each electrolyte's CIS data were fitted with EECs to have a comprehensive understanding of the ion-conducting systems' full electrical properties. The DC conductivity and carrier density increased with increasing GL ratio. With the help of EEC modeling, the transport parameters associated with dissociated ions are calculated. The conductivity measurement was connected to the dielectric characteristics. High dielectric constant and dielectric loss were recorded at low frequencies. The relaxation behaviors of the samples are examined

using loss tangent and electric modulus graphs. The peak detected in the spectra of tanδ and M″ plots and the distribution of data points are asymmetric beside the peaks. This confirms that the movement of ions and their contribution to conductivity belongs to the viscoelastic relaxation type. The high ionic conductivity and improved transport properties (n, μ and D) revealed the suitableness of the films for energy storage device applications.

4. Materials and Methods

4.1. Material Components

PVA (MW 89,000–98,000 g/mol, 99+% hydrolyzed) and chitosan (CS) (MW 310,000–375,000 g/mol, Sigma-Aldrich, St. Louis, MO, USA) are the polymeric materials. Other raw materials employed included sodium bromide (NaBr) (MW 102.89 g/mol, Sigma-Aldrich) salt as a dopant, acetic acid (CH3COOH) solution and distill water as a solvent, and GL (C3H8O3) (MW 92.09 g/mol, Sigma-Aldrich) as a plasticizer. No additional purification was necessary.

4.2. Electrolyte Preparation Using Polymer Blends

Acetic acid solvents were prepared by adding 1 mL of glacial acetic acid into 99 mL of distilled water. 0.5 g of CS was dissolved in 70 mL of the prepared (1%) acetic acid at ambient temperature and 0.5 g of PVA was dissolved in 30 mL distilled water at 90 °C under stirring. After cooling to room temperature, the PVA solution was mixed with dissolved CS. Using a magnetic stirrer, the solution was continuously stirred for 24 h to obtain an identical PVA:CS solution. To make ion-conducting PEs, sodium salt was used. For this purpose, 35 wt.% NaBr salt was added to the PVA:CS solutions under stirring and then addition of varying concentrations (11, 22, 33, 44, and 55 wt.%) of GL as plasticizers into the PVA:CS:NaBr solution were carried out. In order to obtain a dry film free of solvent at room temperature, the solutions were deposited in numerous plastic Petri dishes (8 cm in diameter). This procedure is seen in the Figure 16. The 0.023 mm-thick flexible films were then created.

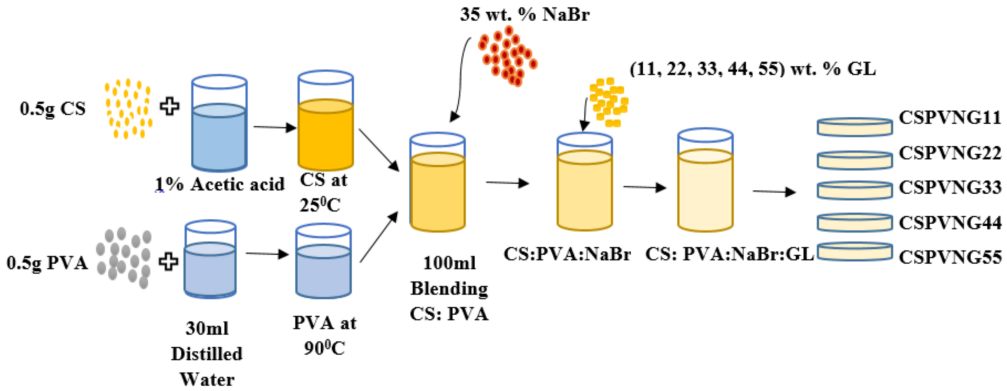

Figure 16. Schematic processes for the fabrication of the plasticized PE samples.

It was determined that CSPVNG0, CSPVNG11, CSPVNG22, CSPVNG33, CSPVNG44, and CSPVNG55 were the appropriate coding for the PVA:CS:NaBr mix systems doped with varied concentrations of GL. Table 5 depicts the film's chemical composition.

Table 5. Solid PE based on PVA:CS:NaBr:GL.

Designation	CS : PVA : NaBr (g)	Glycerol Wt.%	Glycerol (g)
CSPVNG0	(0.5 : 0.5 : 0.538)	0	0
CSPVNG11	(0.5 : 0.5 : 0.538)	11	0.190
CSPVNG22	(0.5 : 0.5 : 0.538)	11	0.4339
CSPVNG33	(0.5 : 0.5 : 0.538)	22	0.758
CSPVNG44	(0.5 : 0.5 : 0.538)	33	1.209
CSPVNG55	(0.5 : 0.5 : 0.538)	44	1.880

4.3. XRD and FTIR Spectra Analysis

Bruker D8 ADVANCE X-ray powder diffractometer (Bruker, Berlin, Germany) with CuK*a* radiation sources (k = 1.54 A°) is used to record XRD patterns of pure and composition polymer films in the region of 10–80° in order to provide information about their crystal structure. The interaction between the composite components was studied using a Perkin Elmer FTIR spectrometer with a range of 500 to 4000 cm^{-1} and a resolution of 2 cm^{-1}.

4.4. Electrical Impedance Spectroscopy (EIS)

Complex impedance spectroscopy may be used to determine the electrical properties of materials and their interaction with electrically conducting electrodes. SPE films were cut into 2 cm diameter compact discs and placed between two stainless steel electrodes under spring pressure as shown in Figure 17.

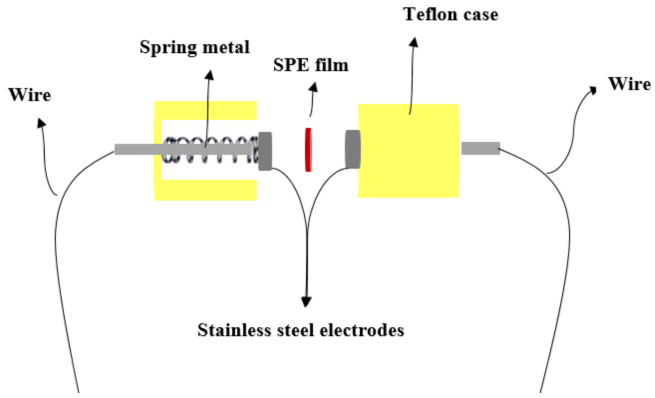

Figure 17. Schematic the stainless-steel electrodes.

HIOKI 3531 Z Hi-tester, linked to a computer, was used to measure the impedance of the films throughout a frequency range of 100 Hz to 2 MHz. Z_r and Z_i are calculated by the software and controlled by it throughout the measuring process. An intersection of the plot and real impedance axis yielded bulk resistance (R_b), and the Z_r and Z_i values were presented as a Nyquist plot. The equation below may be used to determine conductivity [107,108].

In Equation (1), there are three parameters to consider: film thickness (t), bulk resistance (R_b), and active area (A). It is also possible to determine the real and imaginary components of dielectric and electric modulus using Z_r and Z_i by the Equations (9) and (10), (12) and (13), which are based on complex impedance (Z*) [107,108].

Author Contributions: Conceptualization, S.B.A. and M.F.Z.K.; formal analysis, N.M.S.; investigation, N.M.S.; Methodology, N.M.S.; project administration, S.B.A. and M.F.Z.K.; supervision, S.B.A. and M.F.Z.K.; validation, N.M.S., S.B.A. and M.F.Z.K.; writing—original draft, N.M.S.; writing—review & editing, S.B.A. and M.F.Z.K. All authors have read and agreed to the published version of the manuscript.

Funding: This research received no external funding.

Institutional Review Board Statement: Not applicable.

Informed Consent Statement: Not applicable.

Acknowledgments: The authors gratefully acknowledge the financial support for this study from the Ministry of Higher Education and Scientific Research-Kurdish National Research Council (KNRC), Kurdistan Regional Government/Iraq. The financial support from the University of Sulaimani, and Komar University of Science and Technology are greatly appreciated.

Conflicts of Interest: The authors declare that they have no known competing financial interests or personal relationships that could have appeared to influence the work reported in this paper.

References

1. Zhou, Y.; Wang, P.; Ruan, G.; Xu, P.; Ding, Y. Synergistic Effect of P[MPEGMA-IL] Modified Graphene on Morphology and Dielectric Properties of PLA/PCL Blends. *ES Mater. Manuf.* **2020**, *11*, 20–29. [CrossRef]
2. Wang, Z.; He, S.; Nguyen, V.; Riley, K.E. Ionic liquids as "Green solvent and/or electrolyte" for energy interface. *Eng. Sci.* **2020**, *11*, 3–18. [CrossRef]
3. Wang, Y.P.; Gao, X.H.; Li, H.K.; Li, H.J.; Liu, H.G.; Guo, H.X. Effect of active filler addition on the ionic conductivity of PVDF-PEG polymer electrolyte. *J. Macromol. Sci. Part A Pure Appl. Chem.* **2009**, *46*, 461–467. [CrossRef]
4. Angell, C.A. Polymer electrolytes—Some principles, cautions, and new practices. *Electrochim. Acta* **2017**, *250*, 368–375. [CrossRef]
5. Elayappan, V.; Murugadoss, V.; Fei, Z.; Dyson, P.J.; Angaiah, S. Influence of polypyrrole incorporated electrospun poly (vinylidene fluoride-cO–Hexafluoropropylene) nanofibrous composite membrane electrolyte on the photovoltaic performance of dye sensitized solar cell. *Eng. Sci.* **2020**, *10*, 78–84. [CrossRef]
6. Srivastava, M.; Surana, K.; Singh, P.K.; Ch, R. Nickel Oxide embedded with Polymer Electrolyte as Efficient Hole Transport Material for Perovskite Solar Cell. *Eng. Sci.* **2021**, *17*, 216–223. [CrossRef]
7. Wu, X.; Zhong, J.; Zhang, H.; Liu, H.; Mai, J.; Shi, S.; Deng, Q.; Wang, N. Garnet Li7La3Zr2O12 Solid-State Electrolyte: Environmental Corrosion. *Countermeas. Appl. ES Energy Environ.* **2021**, *14*, 22–33. [CrossRef]
8. Maitra, A.; Heuer, A. Understanding correlation effects for ion conduction in polymer electrolytes. *J. Phys. Chem. B* **2008**, *112*, 9641–9651. [CrossRef]
9. Aziz, S.B. Li^+ ion conduction mechanism in poly (ε-caprolactone)-based polymer electrolyte. *Iran. Polym. J.* **2013**, *22*, 877–883. [CrossRef]
10. Hassan, M.; Rafiuddin, R. Ionic Conductivity and Phase Transition Behaviour in 4AgI-(1-)-2CuI System. *Res. Lett. Phys.* **2008**, *2008*, 249402. [CrossRef]
11. Wiśniewski, Z.; Górski, L.; Zasada, D. Investigation of structure and conductivity of superionic conducting materials obtained on the basis of silver iodide. *Acta Phys. Pol. A* **2008**, *113*, 1231–1236. [CrossRef]
12. Mourya, V.K.; Inamdar, N.N. Chitosan-modifications and applications: Opportunities galore. *React. Funct. Polym.* **2008**, *68*, 1013–1051. [CrossRef]
13. Aziz, S.B.; Rasheed, M.A.; Abidin, Z.H.Z. Optical and Electrical Characteristics of Silver Ion Conducting Nanocomposite Solid Polymer Electrolytes Based on Chitosan. *J. Electron. Mater.* **2017**, *46*, 6119–6130. [CrossRef]
14. Aguirre-chagala, Y.E.; Pavón-pérez, L.B.; Altuzar, V.; Domínguez-chávez, J.G.; Muñoz-aguirre, S. Comparative Study of One-Step Cross-Linked Electrospun Chitosan-Based Membranes. *J. Nanomater.* **2017**, *2017*, 1980714. [CrossRef]
15. Fernandes, D.M.; Andrade, J.L.; Lima, M.K.; Silva, M.F.; Andrade, L.H.C.; Lima, S.M.; Hechenleitner, A.A.W.; Pineda, E.A.G. Thermal and photochemical effects on the structure, morphology, thermal and optical properties of PVA/Ni0.04Zn0.96O and PVA/Fe 0.03Zn0.97O nanocomposite films. *Polym. Degrad. Stab.* **2013**, *98*, 1862–1868. [CrossRef]
16. Li, X.; Chen, K.; Ji, X.; Yuan, X.; Lei, Z.; Ullah, M.W.; Xiao, J.; Yang, G. Microencapsulation of poorly water-soluble finasteride in polyvinyl alcohol/chitosan microspheres as a long-term sustained release system for potential embolization applications. *Eng. Sci.* **2021**, *13*, 105–120. [CrossRef]
17. Rao, C.V.S.; Ravi, M.; Raja, V.; Bhargav, P.B.; Sharma, A.K.; Rao, V.V.R.N. Preparation and characterization of PVP-based polymer electrolytes for solid-state battery applications. *Iran. Polym. J.* **2012**, *21*, 531–536. [CrossRef]
18. Nofal, M.M.; Aziz, S.B.; Hadi, J.M.; Karim, W.O.; Dannoun, E.M.A.; Hussein, A.M.; Hussen, S.A. Polymer composites with 0.98 transparencies and small optical energy band gap using a promising green methodology: Structural and optical properties. *Polymers* **2021**, *13*, 1648. [CrossRef] [PubMed]
19. Borgohain, M.M.; Joykumar, T.; Bhat, S.V. Studies on a nanocomposite solid polymer electrolyte with hydrotalcite as a filler. *Solid State Ion.* **2010**, *181*, 964–970. [CrossRef]
20. Kumar, J.; Rodrigues, S.J.; Kumar, B. Interface-mediated electrochemical effects in lithium/polymer-ceramic cells. *J. Power Sources* **2010**, *195*, 327–334. [CrossRef]
21. Aziz, S.B.; Abidin, Z.H.Z. Electrical Conduction Mechanism in Solid Polymer Electrolytes: New Concepts to Arrhenius Equation. *J. Soft Matter* **2013**, *2013*, 323868. [CrossRef]
22. Yusof, Y.M.; Illias, H.A.; Kadir, M.F.Z. Incorporation of NH_4Br in PVA-chitosan blend-based polymer electrolyte and its effect on the conductivity and other electrical properties. *Ionics* **2014**, *20*, 1235–1245. [CrossRef]
23. Buraidah, M.H.; Arof, A.K. Characterization of chitosan/PVA blended electrolyte doped with NH 4I. *J. Non. Cryst. Solids* **2011**, *357*, 3261–3266. [CrossRef]
24. Kadir, M.F.Z.; Majid, S.R.; Arof, A.K. Plasticized chitosan-PVA blend polymer electrolyte based proton battery. *Electrochim. Acta* **2010**, *55*, 1475–1482. [CrossRef]
25. Kadir, M.F.Z.; Arof, A.K. Application of PVA-chitosan blend polymer electrolyte membrane in electrical double layer capacitor. *Mater. Res. Innov.* **2011**, *15* (Suppl. 2), s217–s220. [CrossRef]
26. Hadi, J.M.; Aziz, S.B.; Nofal, M.M.; Hussen, S.A.; Hamsan, M.H.; Brza, M.A.; Abdulwahid, R.T.; Kadir, M.F.Z.; Woo, H.J. Electrical, dielectric property and electrochemical performances of plasticized silver ion-conducting chitosan-based polymer nanocomposites. *Membranes* **2020**, *10*, 151. [CrossRef]
27. Jung, H.-E.; Shin, M. Surface-Roughness-Limited Mean Free Path in Si Nanowire FETs. 2013. Available online: http://arxiv.org/abs/1304.5597 (accessed on 11 May 2015).

28. Ayala, G.; Agudelo, A.; Vargas, R. Effect of glycerol on the electrical properties and phase behavior of cassava starch biopolymers. *Dyna* **2012**, *79*, 138–147.
29. Seoane, N.; Martinez, A.; Brown, A.R.; Asenov, A. Study of surface roughness in extremely small Si nanowire MOSFETs using fully-3D NEGFs. In Proceedings of the 2009 Spanish Conference Electron Devices, Santiago de Compostela, Spain, 11–13 February 2009; pp. 180–183. [CrossRef]
30. Bhargav, P.B.; Sarada, B.A.; Sharma, A.K.; Rao, V.V.R.N. Electrical conduction and dielectric relaxation phenomena of PVA based polymer electrolyte films. *J. Macromol. Sci. Part A Pure Appl. Chem.* **2010**, *47*, 131–137. [CrossRef]
31. Mohan, V.M.; Bhargav, P.B.; Raja, V.; Sharma, A.K.; Rao, V.V.R.N. Optical and electrical properties of pure and doped PEO polymer electrolyte films. *Soft Mater.* **2007**, *5*, 33–46. [CrossRef]
32. Olewnik-Kruszkowska, E.; Gierszewska, M.; Jakubowska, E.; Tarach, I.; Sedlarik, V.; Pummerova, M. Antibacterial films based on PVA and PVA-chitosan modified with poly(hexamethylene guanidine). *Polymers* **2019**, *11*, 2093. [CrossRef] [PubMed]
33. Sharma, P.; Mathur, G.; Goswami, N.; Sharma, S.K.; Dhakate, S.R.; Chand, S.; Mathur, A. Evaluating the potential of chitosan/poly(vinyl alcohol) membranes as alternative carrier material for proliferation of Vero cells. *E-Polymers* **2015**, *15*, 237–243. [CrossRef]
34. Tretinnikov, O.N.; Zagorskaya, S.A. Determination of the degree of crystallinity of poly(Vinyl alcohol) by ftir spectroscopy. *J. Appl. Spectrosc.* **2012**, *79*, 521–526. [CrossRef]
35. Aziz, S.B.; Nofal, M.M.; Ghareeb, H.O.; Dannoun, E.M.A.; Hussen, S.A.; Hadi, J.M.; Ahmed, K.K.; Hussein, A.M. Characteristics of poly(Vinyl alcohol) (PVA) based composites integrated with green synthesized Al^{3+}-metal complex: Structural, optical, and localized density of state analysis. *Polymers* **2021**, *13*, 1316. [CrossRef] [PubMed]
36. Kadir, M.F.Z.; Aspanut, Z.; Majid, S.R.; Arof, A.K. FTIR studies of plasticized poly(vinyl alcohol)-chitosan blend doped with NH4NO3 polymer electrolyte membrane. *Spectrochim. Acta—Part A Mol. Biomol. Spectrosc.* **2011**, *78*, 1068–1074. [CrossRef]
37. Wei, D.; Sun, W.; Qian, W.; Ye, Y.; Ma, X. The synthesis of chitosan-based silver nanoparticles and their antibacterial activity. *Carbohydr. Res.* **2009**, *344*, 2375–2382. [CrossRef] [PubMed]
38. Abdullah, O.G.; Aziz, S.B.; Omer, K.M.; Salih, Y.M. Reducing the optical band gap of polyvinyl alcohol (PVA) based nanocomposite. *J. Mater. Sci. Mater. Electron.* **2015**, *26*, 5303–5309. [CrossRef]
39. Krithiga, N.; Rajalakshmi, A.; Jayachitra, A. Green Synthesis of Silver Nanoparticles Using Leaf Extracts of Clitoria ternatea and Solanum nigrum and Study of Its Antibacterial Effect against Common Nosocomial Pathogens. *J. Nanosci.* **2015**, *2015*, 928204. [CrossRef]
40. Salleh, N.S.; Aziz, S.B.; Aspanut, Z.; Kadir, M.F.Z. Electrical impedance and conduction mechanism analysis of biopolymer electrolytes based on methyl cellulose doped with ammonium iodide. *Ionics* **2016**, *22*, 2157–2167. [CrossRef]
41. Amran, N.N.A.; Manan, N.S.A.; Kadir, M.F.Z. The effect of $LiCF_3SO_3$ on the complexation with potato starch-chitosan blend polymer electrolytes. *Ionics* **2016**, *22*, 1647–1658. [CrossRef]
42. Aziz, S.B. Modifying Poly(Vinyl Alcohol) (PVA) from Insulator to Small-Bandgap Polymer: A Novel Approach for Organic Solar Cells and Optoelectronic Devices. *J. Electron. Mater.* **2016**, *45*, 736–745. [CrossRef]
43. Ricciardi, R.; Auriemma, F.; De Rosa, C.; Lauprêtre, F. X-ray Diffraction Analysis of Poly(vinyl alcohol) Hydrogels, Obtained by Freezing and Thawing Techniques. *Macromolecules* **2004**, *37*, 1921–1927. [CrossRef]
44. Aziz, S.B.; Abidin, Z.H.Z.; Arof, A.K. Effect of silver nanoparticles on the DC conductivity in chitosansilver triflate polymer electrolyte. *Phys. B Condens. Matter* **2010**, *405*, 4429–4433. [CrossRef]
45. Yusuf, S.N.F.; Azzahari, A.D.; Yahya, R.; Majid, S.R.; Careem, M.A.; Arof, A.K. From crab shell to solar cell: A gel polymer electrolyte based on N-phthaloylchitosan and its application in dye-sensitized solar cells. *RSC Adv.* **2016**, *6*, 27714–27724. [CrossRef]
46. Malathi, J.; Kumaravadivel, M.; Brahmanandhan, G.M.; Hema, M.; Baskaran, R.; Selvasekarapandian, S. Structural, thermal and electrical properties of PVA-LiCF3SO3 polymer electrolyte. *J. Non. Cryst. Solids* **2010**, *356*, 2277–2281. [CrossRef]
47. Gasperini, A.; Wang, G.J.N.; Molina-Lopez, F.; Wu, H.C.; Lopez, J.; Xu, J.; Luo, S.; Zhou, D.; Xue, G.; Tok, J.B.H.; et al. Characterization of Hydrogen Bonding Formation and Breaking in Semiconducting Polymers under Mechanical Strain. *Macromolecules* **2019**, *52*, 2476–2486. [CrossRef]
48. Stephan, A.M.; Kumar, T.P.; Kulandainathan, M.A.; Lakshmi, N.A. Chitin-incorporated poly(ethylene oxide)-based nanocomposite electrolytes for lithium batteries. *J. Phys. Chem. B* **2009**, *113*, 1963–1971. [CrossRef]
49. Honary, S.; Orafai, H. The effect of different plasticizer molecular weights and concentrations on mechanical and thermomechanical properties of free films. *Drug Dev. Ind. Pharm.* **2002**, *28*, 711–715. [CrossRef] [PubMed]
50. Honary, S.; Golkar, M. Effect of Polymer Grade and Plasticizer Molecular Weights on Viscoelastic Behavior of Coating Solutions. *Iran. J. Pharm. Res.* **2003**, *2*, 125–127. [CrossRef]
51. Asami, K. Characterization of heterogeneous systems by dielectric spectroscopy. *Prog. Polym. Sci.* **2002**, *27*, 1617–1659. [CrossRef]
52. Polu, A.R.; Kumar, R. Impedance spectroscopy and FTIR studies of PEG—Based polymer electrolytes. *E-J. Chem.* **2011**, *8*, 347–353. [CrossRef]
53. Mahato, D.K.; Dutta, A.; Sinha, T.P. Impedance spectroscopy analysis of double perovskite Ho_2NiTiO_6. *J. Mater. Sci.* **2010**, *45*, 6757–6762. [CrossRef]
54. Fortunato, R.; Branco, L.C.; Afonso, C.A.M.; Benavente, J.; Crespo, J.G. Electrical impedance spectroscopy characterisation of supported ionic liquid membranes. *J. Memb. Sci.* **2006**, *270*, 42–49. [CrossRef]

55. Aziz, S.B.; Abdullah, R.M. Crystalline and amorphous phase identification from the tanδ relaxation peaks and impedance plots in polymer blend electrolytes based on [CS:AgNt]x:PEO(x-1) ($10 \leq x \leq 50$). *Electrochim. Acta* **2018**, *285*, 30–46. [CrossRef]
56. Benavente, J.; García, J.M.; Riley, R.; Lozano, A.E.; De Abajo, J. Sulfonated poly(ether ether sulfones): Characterization and study of dielectrical properties by impedance spectroscopy. *J. Memb. Sci.* **2000**, *175*, 43–52. [CrossRef]
57. Benavente, J.; Zhang, X.; Valls, R.G. Modification of polysulfone membranes with polyethylene glycol and lignosulfate: Electrical characterization by impedance spectroscopy measurements. *J. Colloid Interface Sci.* **2005**, *285*, 273–280. [CrossRef] [PubMed]
58. Aziz, S.B.; Abdullah, R.M.; Rasheed, M.A.; Ahmed, H.M. Role of Ion Dissociation on DC Conductivity and Silver Nanoparticle Formation in PVA:AgNt Based Polymer Electrolytes: Deep Insights to Ion Transport Mechanism. *Polymers* **2017**, *9*, 338. [CrossRef] [PubMed]
59. Jacob, M.M.E.; Prabaharan, S.R.S.; Radhakrishna, S. Effect of PEO addition on the electrolytic and thermal properties of PVDF-LiClO4 polymer electrolytes. *Solid State Ion.* **1997**, *4*, 267–276. [CrossRef]
60. Qian, H.; Wang, Y.; Fang, Y.; Gu, L.; Lu, R.; Sha, J. High-performance ZnO nanowire field-effect transistor with forming gas treated SiO2 gate dielectrics. *J. Appl. Phys.* **2015**, *117*, 164308. [CrossRef]
61. Shukur, M.F.; Ithnin, R.; Kadir, M.F.Z. Electrical characterization of corn starch-LiOAc electrolytes and application in electrochemical double layer capacitor. *Electrochim. Acta* **2014**, *136*, 204–216. [CrossRef]
62. Teo, L.P.; Buraidah, M.H.; Nor, A.F.M.; Majid, S.R. Conductivity and dielectric studies of Li_2SnO_3. *Ionics* **2012**, *18*, 655–665. [CrossRef]
63. Asnawi, A.S.F.M.; Aziz, S.B.; Brevik, I.; Brza, M.A.; Yusof, Y.M.; Alshehri, S.M.; Ahamad, T.; Kadir, M.F.Z. The Study of Plasticized Sodium Ion Conducting Polymer Blend Electrolyte Membranes Based on Chitosan/Dextran Biopolymers: Ion Transport, Structural, Morphological and Potential Stability. *Polymers* **2021**, *13*, 383. [CrossRef]
64. Paluch, M.; Ostrowska, J.; Tyński, P.; Sadurski, W.; Konkol, M. Structural and Thermal Properties of Starch Plasticized with Glycerol/Urea Mixture. *J. Polym. Environ.* **2021**, *30*, 728–740. [CrossRef]
65. Kobayashi, K.; Pagot, G.; Vezzù, K.; Bertasi, F.; di Noto, V.; Tominaga, Y. Effect of plasticizer on the ion-conductive and dielectric behavior of poly(ethylene carbonate)-based Li electrolytes. *Polym. J.* **2021**, *53*, 149–155. [CrossRef]
66. Dinoto, V.; Negro, E.; Lavina, S.; Vittadello, M. Hybrid inorganiC–Organic polymer electrolytes. In *Polymer Electrolytes*; Woodhead Publishing: Sawston, UK, 2010; pp. 219–277. [CrossRef]
67. Muldoon, J.; Bucur, C.B.; Boaretto, N.; Gregory, T.; di Noto, V. Polymers: Opening doors to future batteries. *Polym. Rev.* **2015**, *55*, 208–246. [CrossRef]
68. di Noto, V.; Lavina, S.; Giffin, G.A.; Negro, E.; Scrosati, B. Polymer electrolytes: Present, past and future. *Electrochim. Acta* **2011**, *57*, 4–13. [CrossRef]
69. Arof, A.K.; Amirudin, S.; Yusof, S.Z.; Noor, I.M. A method based on impedance spectroscopy to determine transport properties of polymer electrolytes. *Phys. Chem. Chem. Phys.* **2014**, *16*, 1856–1867. [CrossRef] [PubMed]
70. Shukur, M.F.; Ithnin, R.; Kadir, M.F.Z. Electrical properties of proton conducting solid biopolymer electrolytes based on starch-chitosan blend. *Ionics* **2014**, *20*, 977–999. [CrossRef]
71. Yusof, Y.M.; Shukur, M.F.; Hamsan, M.H.; Jumbri, K.; Kadir, M.F.Z. Plasticized solid polymer electrolyte based on natural polymer blend incorporated with lithium perchlorate for electrical double-layer capacitor fabrication. *Ionics* **2019**, *25*, 5473–5484. [CrossRef]
72. Asnawi, A.S.F.M.; Aziz, B.S.; Nofal, M.M.; Hamsan, M.H.; Brza, M.A.; Yusof, Y.M.; Abdilwahid, R.T.; Muzakir, S.K.; Kadir, M.F.Z. Glycerolized Li^+ Ion Conducting Chitosan-Based Polymer Electrolyte for Energy Storage EDLC Device Applications with Relatively High Energy Density. *Polymers* **2020**, *12*, 1433. [CrossRef] [PubMed]
73. Lu, J.; Deng, Y.; Song, J.; Hu, Y.; Deng, Z.; Cui, Q.; Lou, Z. Role of Hydroxyl on Conductivity Switching of Poly(ethylene oxide)/TiO_2 Electrical Bistable Devices. *Phys. Status Solidi Appl. Mater. Sci* **2019**, *216*, 1900443. [CrossRef]
74. Müller, C.M.O.; Yamashita, F.; Laurindo, J.B. Evaluation of the effects of glycerol and sorbitol concentration and water activity on the water barrier properties of cassava starch films through a solubility approach. *Carbohydr. Polym.* **2008**, *72*, 82–87. [CrossRef]
75. Impedance Spectroscopy. In *Gas Adsorption Equilibria*; Springer: Boston, MA, USA, 2005; pp. 287–357. [CrossRef]
76. Aziz, S.B. Role of dielectric constant on ion transport: Reformulated Arrhenius equation. *Adv. Mater. Sci. Eng.* **2016**, *2016*, 2527013. [CrossRef]
77. Okutan, M.; Şentürk, E. β Dielectric relaxation mode in side-chain liquid crystalline polymer film. *J. Non. Cryst. Solids* **2008**, *354*, 1526–1530. [CrossRef]
78. Sun, L.; Liang, L.; Shi, Z.; Wang, H.; Xie, P.; Dastan, D.; Sun, K.; Fan, R. Optimizing strategy for the dielectric performance of topological-structured polymer nanocomposites by rationally tailoring the spatial distribution of nanofillers. *Eng. Sci.* **2020**, *12*, 95–105. [CrossRef]
79. Pradhan, D.K.; Choudhary, R.N.P.; Samantaray, B.K. Studies of dielectric relaxation and AC conductivity behavior of plasticized polymer nanocomposite electrolytes. *Int. J. Electrochem. Sci.* **2008**, *3*, 597–608.
80. Marzantowicz, M.; Dygas, J.R.; Krok, F.; Łasińska, A.; Florjańczyk, Z.; Zygadło-Monikowska, E. In situ microscope and impedance study of polymer electrolytes. *Electrochim. Acta* **2006**, *51*, 1713–1727. [CrossRef]
81. Marzantowicz, M.; Dygas, J.R.; Krok, F.; Łasińska, A.; Florjańczyk, Z.; Zygadło-Monikowska, E.; Affek, A. Crystallization and melting of PEO:LiTFSI polymer electrolytes investigated simultaneously by impedance spectroscopy and polarizing microscopy. *Electrochim. Acta* **2005**, *50*, 3969–3977. [CrossRef]

82. Aziz, S.B.; Abidin, Z.H.Z. Electrical and morphological analysis of chitosan:AgTf solid electrolyte. *Mater. Chem. Phys.* **2014**, *144*, 280–286. [CrossRef]
83. Hurd, J.A.; Vaidhyanathan, R.; Thangadurai, V.; Ratcliffe, C.I.; Moudrakovski, I.L.; Shimizu, G.K.H. Anhydrous proton conduction at 150 °C in a crystalline metal-organic framework. *Nat. Chem.* **2009**, *1*, 705–710. [CrossRef]
84. Bureekaew, S.; Horike, S.; Higuchi, M.; Mizuno, M.; Kawamura, T.; Tanaka, D.; Yanai, N.; Kitagawa, S. One-dimensional imidazole aggregate in aluminium porous coordination polymers with high proton conductivity. *Nat. Mater.* **2009**, *8*, 831–836. [CrossRef]
85. Nicolau, A.; Nucci, A.M.; Martini, E.M.A.; Samios, D. Electrical impedance spectroscopy of epoxy systems II: Molar fraction variation, resistivity, capacitance and relaxation processes of 1,4-butanediol diglycidyl ether/succinic anhydride and triethylamine as initiator. *Eur. Polym. J.* **2007**, *43*, 2708–2717. [CrossRef]
86. Wang, W.; Alexandridis, P. Composite Polymer Electrolytes: Nanoparticles Affect Structure and Properties. *Polymers* **2016**, *8*, 387. [CrossRef] [PubMed]
87. Aziz, S.B.; Abdullah, O.G.; Rasheed, M.A. Structural and electrical characteristics of PVA:NaTf based solid polymer electrolytes: Role of lattice energy of salts on electrical DC conductivity. *J. Mater. Sci. Mater. Electron.* **2017**, *28*, 12873–12884. [CrossRef]
88. Marzantowicz, M.; Dygas, J.R.; Krok, F.; Florjaczyk, Z.; Zygado-Monikowska, E. Conductivity and dielectric properties of polymer electrolytes PEO:LiN(CF3SO2)2 near glass transition. *J. Non. Cryst. Solids* **2007**, *353*, 4467–4473. [CrossRef]
89. Mohomed, K.; Moussy, F.; Harmon, J.P. Dielectric analyses of a series of poly(2-hydroxyethyl methacrylate-co-2,3-dihydroxypropyl methacylate) copolymers. *Polymer* **2006**, *47*, 3856–3865. [CrossRef]
90. Kamal, A.; Rafiq, M.A.; Rafiq, M.N.; Usman, M.; Waqar, M.; Anwar, M.S. Structural and impedance spectroscopic studies of CuO-doped (K0.5Na0.5Nb0.995Mn0.005O3) lead-free piezoelectric ceramics. *Appl. Phys. A Mater. Sci. Process.* **2016**, *122*, 1037. [CrossRef]
91. Rayssi, C.; El Kossi, S.; Dhahri, J.; Khirouni, K. Frequency and temperature-dependence of dielectric permittivity and electric modulus studies of the solid solution Ca0.85Er0.1Ti1-: XCo4 x /3O3 ($0 \leq x \leq 0.1$). *RSC Adv.* **2018**, *8*, 17139–17150. [CrossRef]
92. Smaoui, H.; Arous, M.; Guermazi, H.; Agnel, S.; Toureille, A. Study of relaxations in epoxy polymer by thermally stimulated depolarization current (TSDC) and dielectric relaxation spectroscopy (DRS). *J. Alloys Compd.* **2010**, *489*, 429–436. [CrossRef]
93. Agrawal, S.L.; Singh, M.; Asthana, N.; Dwivedi, M.M.; Pandey, K. Dielectric and ion transport studies in [PVA: $LiC_2H_3O_2$]: $Li_2Fe_5O_8$ polymer nanocomposite electrolyte system. *Int. J. Polym. Mater. Polym. Biomater.* **2011**, *60*, 276–289. [CrossRef]
94. Ayesh, A.S. Dielectric relaxation and thermal stability of polycarbonate doped with $MnCl_2$ salt. *J. Thermoplast. Compos. Mater.* **2008**, *21*, 309–322. [CrossRef]
95. Ayesh, A.S. Electrical and optical characterization of PMMA doped with Y 0.0025Si0.025Ba0.9725 (Ti(0.9)Sn0.1)O3 ceramic. *Chin. J. Polym. Sci.* **2010**, *28*, 537–546. [CrossRef]
96. Aziz, S.B.; Karim, W.O.; Brza, M.A.; Abdulwahid, R.T.; Saeed, S.R.; Al-Zangana, S.; Kadir, M.F.Z. Ion Transport Study in CS: POZ Based Polymer Membrane Electrolytes Using Trukhan Model. *Int. J. Mol. Sci.* **2019**, *20*, 5265. [CrossRef] [PubMed]
97. Mohomed, K.; Gerasimov, T.G.; Moussy, F.; Harmon, J.P. A broad spectrum analysis of the dielectric properties of poly(2-hydroxyethyl methacrylate). *Polymer* **2005**, *46*, 3847–3855. [CrossRef]
98. Gommans, H.H.P. Charge Transport and Interface Phenomena in Semiconducting Polymers. Ph.D.Thesis, Technische Universiteit Eindhoven, Eindhoven, The Netherlands, September 2005.
99. Barker, R.E. Mobility and Conduction of Ions in and into Polymeric Solids. *Pure & Appi. Chem.* **1976**, *46*, 157–170. [CrossRef]
100. Rozanskia, S.A.; Kremer, F.; Kijberle, P. Relaxation and charge transport in mixtures of zwitterionic polymers and inorganic salts. *Macromol. Chem. Phys.* **1995**, *890*, 877–890. [CrossRef]
101. Bassiouni, M.E.; Al-shamy, F.; Madi, N.K.; Kassem, M.E. Temperature and electric field effects on the dielectric dispersion of modified polyvinyl chloride. *Mater. Lett.* **2003**, *57*, 1595–1603. [CrossRef]
102. Hema, M.; Selvasekerapandian, S.; Sakunthala, A.; Arunkumar, D.; Nithya, H. Structural, vibrational and electrical characterization of PVA-NH4Br polymer electrolyte system. *Phys. B Condens. Matter* **2008**, *403*, 2740–2747. [CrossRef]
103. Yang, J.; Meng, X.J.; Shen, M.R.; Fang, L.; Wang, J.L.; Lin, T.; Sun, J.L.; Chu, J.H. Hopping conduction and low-frequency dielectric relaxation in 5 mol % Mn doped (Pb, Sr) TiO_3 films. *J. Appl. Phys.* **2008**, *104*, 113. [CrossRef]
104. Migahed, M.D.; Ishra, M.; Fahmy, T.; Barakat, A. Electric modulus and AC conductivity studies in conducting PPy composite films at low temperature. *J. Phys. Chem. Solids* **2004**, *65*, 1121–1125. [CrossRef]
105. Ravi, M.; Pavani, Y.; Kumar, K.K.; Bhavani, S.; Sharma, A.K.; Rao, V.V.R.N. Studies on electrical and dielectric properties of PVP: $KBrO_4$ complexed polymer electrolyte films. *Mater. Chem. Phys.* **2011**, *130*, 442–448. [CrossRef]
106. Bhadra, S.; Singha, N.K.; Khastgir, D. Dielectric properties and EMI shielding efficiency of polyaniline and ethylene 1-octene based semi-conducting composites. *Curr. Appl. Phys.* **2009**, *9*, 396–403. [CrossRef]
107. Daniel, R.; Janet Priscilla, S.; Karthikeyan, S.; Selvasekarapandian, S.; Madeswaran, S.; Sivaji, K. Structural and Electrical Studies on PVP—Pan Blend Polymer System for Energy Storage Devices. *Int. J. Curr. Res. Rev.* **2018**, *10*, 19–24. [CrossRef]
108. Ibrahim, S.; Yasin, S.M.M.; Nee, N.M.; Ahmad, R.; Johan, M.R. Conductivity and dielectric behaviour of PEO-based solid nanocomposite polymer electrolytes. *Solid State Commun.* **2012**, *152*, 426–434. [CrossRef]